

Quantum criticality in photorefractive optics: vortices in laser beams and antiferromagnets

Mihailo Čubrović* and Milan Petrović

Institute of Physics, P. O. B. 57, 11001 Belgrade, Serbia

(Dated: September 1, 2022)

We study vortex patterns in a prototype nonlinear optical system: counterpropagating laser beams in a photorefractive crystal, with or without the background photonic lattice. The vortices are effectively planar and described by the winding number and the "flavor" index, stemming from the fact that we have two parallel beams propagating in opposite directions. The problem is amenable to the methods of statistical field theory and generalizes the Berezinsky-Kosterlitz-Thouless transition of the XY model to the "two-flavor" case. In addition to the familiar conductor and insulator phases, we also have the perfect conductor (vortex proliferation in both beams/"flavors") and the frustrated insulator (energy costs of vortex proliferation and vortex annihilation balance each other). In the presence of disorder in the background lattice, a novel phase appears which shows long-range correlations and absence of long-range order, thus being analogous to spin glasses. An important benefit of this approach is that qualitative behavior of patterns can be known without intensive numerical work over large areas of the parameter space. More generally, we would like to draw attention to connections between the (classical) pattern-forming systems in photorefractive optics and the methods of (quantum) condensed matter and field theory: on one hand, we use the field-theoretical methods (renormalization group, replica formalism) to analyze the patterns; on the other hand, the observed phases are analogous to those seen in magnetic systems, and make photorefractive optics a fruitful testing ground for condensed matter systems. As an example, we map our system to a doped $O(3)$ antiferromagnet with \mathbb{Z}_2 defects, which has the same structure of the phase diagram.

I. INTRODUCTION

Nonlinear and pattern-forming systems [1–3] have numerous analogies with strongly correlated systems encountered in condensed matter physics [4, 5], and on the methodological level they are both united through the language of field theory, which has become the standard language to describe strongly correlated electrons [6, 7] as well as nonlinear dynamical systems [8]. In the field of pattern formation, some connections to condensed matter systems have been observed, see e.g. [4]. However, this topic is far from exhausted and we feel many analogies between quantum many-body systems and pattern-formation dynamics remain unexplored and unexploited. In particular, nonlinear optical systems and photonic lattices are flexible and relatively cheap to build [3] and they can be used to "simulate" a broad spectrum of phenomena concerning band structure, spin ordering and conduction in strongly correlated electron systems; some of the work in this direction can be found in [9, 10].

Our goal is to broaden the connections between the strongly correlated systems and nonlinear optics and to put to work the mighty apparatus of field theory to study the pattern dynamics and statistics in a nonlinear optical system. We find that the pattern dynamics in certain cases shows critical behavior which is analogous to phenomena seen in magnetic systems. To that end, we use the formalism of perturbative field theory and renormalization group analysis, which to the best of our knowledge were not so far applied to nonlinear optical systems. We will also establish a connection to a certain antiferromagnetic model which is encountered in the study of strongly correlated electron systems. The analogy is not just qualitative: we will construct the phase diagrams of both systems and find they have the same structure. Introducing disorder into the system further enriches the physics, and it is physically motivated: in optics, disorder is rooted in the imperfections of the photonic lattice, and in magnetic systems it comes from the quenched spin impurities which are regularly found in realistic samples. It turns out that in both cases a glassy phase arises. This is another important research topic and it is again appealing to realize glasses in photonic lattice systems, where the parameters are easy to tune.

*Electronic address: mcubrovic@gmail.com

A. On defects and vortices

The key phenomenon which governs the phenomenology of the systems studied is the existence of topologically nontrivial solutions or *topological solitons* [11]: these are the solutions which map the physical boundary of the system to the whole configuration space of the field, so one explores all field configurations by "going around the system". For example, in a two-dimensional (planar) system with $U(1)$ phase symmetry, the configuration space is a circle, the boundary of the space is a circle at infinity, and the topological soliton spans the whole configuration space (the phase circle as the group manifold of $U(1)$) one or more times upon winding the circular boundary which encloses the soliton. Of course, this is the vortex – the most famous and best studied topological configuration. Similar logic leads to the classification of topological defects of other, more complicated symmetry groups. A potential source of confusion is that in nonlinear dynamics and theory of partial differential equations, the "integrable" solutions, i.e. linearly (often also nonlinearly) stable solutions which can be obtained by inverse scattering or similar methods and which propagate through each other without interacting, are also called solitons, or more precisely *dynamical solitons*. Dynamical solitons in nonlinear optics are a celebrated and well-studied topic [12], they show an amazing variety of patterns and phenomena like localization, Floquet states [9], etc. But they in general do not have a topological charge. In contrast, topological solitons carry a topological charge (winding number for vortices) and their stability is rooted in topological protection (conservation of topological charge).

The study of vortices started with the classical work of Abrikosov [13] in three spatial dimensions. It establishes the existence of vortex line configurations of the phase of the wavefunction and shows that vortices are stable when the phase symmetry is broken by magnetic field. Famously, vortices may coexist with the superconducting order ($U(1)$ symmetry breaking) in type-II superconductors or exist only in the normal phase, upon destroying the superconductivity (type I). The primary example in two spatial dimensions is the vortex unbinding phase transition of infinite order found by Berezinsky, Kosterlitz and Thouless for the planar XY model [18]. The formal difference between the two- and three-dimensional vortices is that the latter give rise to an emergent gauge field; this does not happen in the XY-like system in two dimensions [14]. While the nonlinear optical system we study is three-dimensional, its geometry and relaxational dynamics make it natural to treat it as a $2 + 1$ -dimensional system (while time is a parameter). We therefore have a similar situation to the XY model: point-like vortices in the plane (and no gauge field).

Vortex matter is known to emerge in liquid helium [15], Bose-Einstein condensates [16] and magnetic systems [17]. The basic mechanisms of vortex dynamics are thus well known. However, novel physics can arise if the system has multiple components and each of them can form vortices which mutually interact. This is precisely our situation – we have a system of two laser beams propagating in opposite directions, and we will compare it to a two-component antiferromagnet. So far, such situations have been explored in multi-component superconductors [19] which have attracted some attention, as they can be realized in magnesium diboride [20]. But these are again bulk systems, not planar. Vortices in planar multi-component systems have not been very popular, except for the two-component Bose-Einstein condensates of [22], which were found to exhibit complex vortex dynamics; in these systems, contrary to our case, the two components have an explicit attractive interaction, unlike our case where they interact indirectly, by coupling to the total light intensity (of both components).

B. The object of our study

In this paper we will study critical behavior of topological configurations (vortices and vortex lattices) in a specific and experimentally realizable nonlinear optical system: laser beams counterpropagating (CP) through a photorefractive (PR) crystal. This means we have an elongated PR crystal (with one longitudinal and two transverse dimensions) and two laser beams shone onto each end. We thus effectively have two fields, one forward-propagating and one backward propagating. The optical response of the crystal depends nonlinearly on the *total* intensity of both beams, which means the beams effectively interact with each other. This system has been thoroughly investigated for phenomena such as dynamical solitons [12, 23, 28], vortex stability on the photonic lattice [25, 27, 29–32] and global rotation [26]. We will see that the CP beams are an analogue of the two-component planar antiferromagnet (AF), which can further be related to some realistic strongly-correlated materials [33, 43, 45]. The two beams now become two sublattices which interact through a lattice deformation or external field. The PR crystal is elongated and the axial propagation direction has the role of time, which is compactified to a finite radius, the length of the crystal. For the antiferromagnet, the third axis is the usual imaginary time compactified to the radius $1/T$, i.e. inverse temperature. We will see that such connections between PR nonlinear optics and spin systems are many, and have been scarcely explored so far. It is therefore a promising field for future work, especially since laser beams in PR crystals are easy to tune in experiment, have been studied for quite some time and are cheap to build [3]. Both systems contain vortices as topological defects, i.e. solutions with integer topological charge. In the PR optical system, vortices arise as a consequence of the $U(1)$ symmetry of the electromagnetic field. In antiferromagnets we consider, the $O(3)$ symmetry

of the antiferromagnet gives rise to \mathbb{Z}_2 -charged defects, which exhibit the same interactions as the vortices.

In the PR counterpropagating beam system, we will discuss mainly the vortices but in order to do that we need to consider first the topologically trivial patterns and construct a perturbation theory for them. This does not mean that these non-topological patterns are "perturbative solutions" in the usual sense – this system exhibits dynamical solitons, and they are by definition non-perturbative solutions in the sense that they cannot be continued to plane waves. But if we start from a dynamical soliton then we can construct a perturbation theory of fluctuations around this pattern. This is a basic exercise which however was not done so far. It is this field-theoretical approach that allows us to see optical solitons as vacua (classical solutions) of an effective (macroscopic) XY-spin field in a magnetic material. Our aim is to introduce and popularize this approach which deepens the connection of nonlinear optics to other areas of physics. It also allows us to avoid painful and extensive numerics – analytical construction of the phase diagram tells us which patterns can in principle be expected in different corners of the parameter space. By "blind" numerical approach this result could only be found through many runs of the numerics.

In the antiferromagnetic spin system the non-topological excitations are simple – they are spin waves, perturbed away from the noninteracting solution by the quartic terms in the potential. There are no dynamical solitons. But we will see that topological excitations lead to a phase diagram which, after reasonable approximations, can be *exactly* mapped to the phase diagram of the photorefractive crystal. The reason is that both can be reduced to an effective Hamiltonian for a *two-component* vortex system, i.e., every vortex has two charges, or two "flavors". In the photorefractive crystal it happens naturally, as there are two beams, forward- and backward propagating. In the Heisenberg antiferromagnet it is less obvious, and is a crucial consequence of the collinearity of the spin pattern. We will focus on common properties of the two systems and show how the multi-component vortex system gives rise to long-range order. Different ordered phases are separated by quantum phase transitions, phase transitions driven by the quantum fluctuations instead of temperature. In both systems we will consider also the influence of the temperature, however in the optical system there is no true temperature and the "thermal" properties are to be understood as stemming from varying the crystal length L (which corresponds to the inverse temperature).

1. On disorder

It is known that impurities pin the vortices and stabilize them. This leads to frozen dynamics even though no symmetry is broken, the phenomenon usually associated with glasses. In simple systems such as Ising model with disorder one generically has two phases: the disordered (paramagnetic) phase remains and the ordered (magnetic) phase is replaced by a regime with algebraic correlations and no true order. In many cases, such phases are called glasses. The exact definition of a glass is lacking; normally, they show (i) long-range correlations (ii) absence of order, i.e. of nonzero macroscopic order parameter (iii) "frozen dynamics", i.e. free energy landscape with numerous local minima in which the system can spend a long time [36, 37]. While the most popular example are probably spin glasses in models such as Sheringtin-Kirkpatrick and Edwards-Anderson model, glasses are also known to appear in the XY model with disorder in two dimensions, which was studied in [39–41] among other papers. The details differ depending on how the disorder is implemented but the two-phase system (paramagnetic i.e. disordered, and glass) is ubiquitous. In the two-component version, the phase diagram becomes richer, and we identify both a glassy phase (satisfying the above requirements), the insulator (disordered) phase and a few other phases. Here the relation to magnetic systems in condensed matter physics is very inspiring, since a number of complex materials show different ordering mechanisms (spin and charge density waves, superconductivity, etc) in parallel with significant influence of disorder. Just as in the disorder-free case, we are particularly interested in possible spin-glass phenomena in doped insulating $O(3)$ antiferromagnets [43–47] and in the last section we will discuss also the spin-glass phase in such systems.

C. The plan of the paper

The structure of the paper is as follows. In the next section we describe the dynamical system which lies at the core of this paper: counterpropagating laser beams in a photorefractive crystal. We give the equations of motion and repackage them in the Lagrangian form and in field-theory language. In section III we study the vortex dynamics: we construct the vortex Hamiltonian, classify the order parameters and construct the mean-field phase diagram. Then we study the renormalization group (RG) flow and obtain a refined phase diagram. Finally, we discuss the important question of how to recognize the various phases in experiment: what do the intensity patterns look like and how they depend on the tunable parameters. Section IV brings the same study for the system with disorder. After describing the disordered system, we perform the replica trick for the disordered vortex Hamiltonian and solve the saddle-point equations to identify the phases and order parameters, again refining the results with RG calculations. The fifth section takes a look at a doped collinear antiferromagnet, a model frequently encountered in the description of many

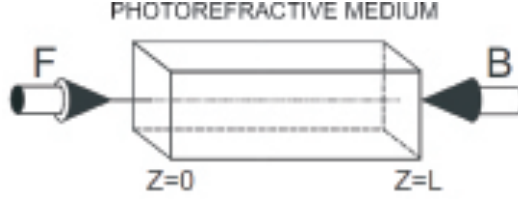


FIG. 1: Sketch of the experimental setup for the study of the CP beams in the PR crystal. The crystal has the shape of a parallelepiped, and the beams propagate along the longitudinal, z -axis: the F -beam from $z = 0$ to $z = L$, and the B -beam the other way round. The intensity patterns are observed at the transverse faces of the crystal, at $z = 0$ and $z = L$.

strongly coupled materials, and shows how the dynamics of topological solitons is again described by a two-flavor vortex Hamiltonian. We discuss the relation between the phase diagrams of the two systems and the possibilities of modeling the condensed matter systems experimentally by the means of photorefractive optics. The last section sums up the conclusions. In the Appendix we formulate a perturbation theory which can be used for stability analysis of (non-topological) patterns in the PR crystal. Although somewhat peripheral to our main topic, it is a good illustration of our approach and also will provide some explanations on the geometry and symmetry of vortex patterns.

II. THE MODEL OF COUNTERPROPAGATING BEAMS IN THE PHOTOREFRACTIVE CRYSTAL

We consider a photorefractive crystal of length L irradiated by two laser beams. The beams are paraxial and propagate head-on from the opposite faces of the crystal in the z -direction. Photorefractive crystals induce self-focusing of the beams – the vacuum (linear) wave equation is modified by the addition of a friction-like term, so the diffusion of the light intensity (the broadening of the beam) is balanced out by the convergence of the beam onto an “attractor region”. The net result is the balance between the dissipative and scattering effects, allowing for stable patterns to form. The physical ground for this is the redistribution of the charges in the crystal due to the Kerr effect. The nonlinearity, i.e. the response of the crystal to the laser light is contained in the change of the refraction index which is determined by the local charge density. A sketch of the system is given in Fig. 1. The laser beam can be given any desirable pattern of both intensity and phase. In particular, we can create vortices (winding of the phase) making use of the phase masks [3] or other, more modern ways.

Assuming the electromagnetic field of the form $\mathbf{E} = e^{i\omega t + i\mathbf{q}\mathbf{r}} (Fe^{ikz} + Be^{-ikz})$, we can write equations for the so-called envelopes F and B of the forward- and backward propagating beams along the z -axis (the frequency, transverse and longitudinal momentum are denoted respectively by ω, \mathbf{q}, k). The wave equations for F and B are now:

$$\pm i\partial_z \Psi_{\pm}(z; x, y, t) + \Delta \Psi_{\pm}(z; x, y, t) = \Gamma E(z; x, y, t) \Psi_{\pm}(z; x, y, t), \quad (1)$$

where the plus and minus signs on the left-hand side stand for the forward- and backward-propagating component of the beam amplitude doublet $\Psi \equiv (\Psi_+, \Psi_-) \equiv (F, B)$, and Γ is the dimensionless PR coupling constant. The two beams (flavors of the field Ψ) will from now on be denoted either by F/B or more often by Ψ_{\pm} . We will use α as the general flavor index for summation, e.g. $\Psi_{1\alpha} \Psi_{2\alpha} = \Psi_{1+} \Psi_{2+} + \Psi_{1-} \Psi_{2-}$. The charge field E on the right-hand side of the equation is the electric field sourced by the charges in the crystal (i.e., it does not include the external electric field of the beams). Its evolution is well represented by a relaxation-type equation [12]:

$$\frac{\tau}{1 + I(z; x, y, t)} \partial_t E(z; x, y, t) + E(z; x, y, t) = -\frac{I(z; x, y, t)}{1 + I(z; x, y, t)}. \quad (2)$$

Here, $I \equiv I_{\Psi} + I_x$ is the total light intensity at a given point, $I_{\Psi} \equiv |F|^2 + |B|^2$ is the beam intensity and I_x the intensity of the fixed background. The meaning of I_x is that the crystal is all the time irradiated by some constant light source, independent of the counter-propagating beams with envelopes F, B . We will usually take a periodic lattice as the background, allowing also for the defects (missing cells) in the lattice when studying the effects of disorder. The relaxation time is τ . The time derivative $\partial_t E$ is divided by $1 + I$, meaning that the polarizability of the crystal depends on the total light intensity: strongly irradiated regions react faster. This equation has no microscopic basis, it is completely phenomenological, but it represents excellently the experimental results.

For slow time evolution (in absence of pulses), we can Laplace-transform the equation (2) in time ($E(t) \mapsto E(u) = \int_0^{\infty} dt e^{-ut} E(t)$) to get the algebraic relation

$$E(z; x, y, u) = -\frac{\Psi^{\dagger} \Psi + I_x - \tau E_0}{1 + \tau u + I_x + \Psi^{\dagger} \Psi} = -1 + \frac{1 + \tau u + \tau E_0}{1 + \tau u + I_x + \Psi^{\dagger} \Psi}. \quad (3)$$

The original system (1) can now be described by the Lagrangian:

$$\mathcal{L} = i\Psi^\dagger \sigma_3 \partial_z \Psi - |\nabla \Psi|^2 + \Gamma \Psi^\dagger \Psi - \Gamma(1 + \tau E_0 + \tau u) \log(1 + \tau u + I_x + \Psi^\dagger \Psi), \quad (4)$$

where σ_3 is the Pauli matrix $\sigma_3 = \text{diag}(1, -1)$. One can introduce the effective potential

$$V_{\text{eff}}(\Psi^\dagger, \Psi) = -\Gamma \log \frac{e^{\Psi^\dagger \Psi}}{(1 + \tau u + I_x + \Psi^\dagger \Psi)^{1+\tau(E_0+u)}}, \quad (5)$$

so we can write the Lagrangian as $\mathcal{L} = i\Psi^\dagger \sigma_3 \partial_z \Psi - |\nabla \Psi|^2 - V_{\text{eff}}(\Psi^\dagger, \Psi)$. This is the Lagrangian of a field theory in $2+1$ dimensions $(x, y; z)$, where the role of time is played by the longitudinal distance z , and the physical time t (or u upon the Laplace transform) is a parameter. Importantly, z has a finite domain $(0 \leq z \leq L)$, similar to the Euclidean time in field theories at finite temperature. This allows us to identify the crystal length L with inverse temperature $1/T$. The zero-temperature limit thus corresponds to the infinite crystal and therefore is not physically realizable but is a useful idealization: some order parameters only become stable at infinite propagation length.

Our main story is now the nature and interactions of the topologically nontrivial excitations in the system (4). A task which is in a sense more basic, the analysis of the topologically trivial vacua of (4) and perturbative calculation of their stability, is not of our primary interest now, in part because this was largely accomplished by other methods in [23, 28]. We nevertheless give a quick account in the Appendix; first, because we will need one result (the expansion in the vicinity of the mean-field solution) to derive the vortex Hamiltonian, and second, to give another example of applying the field-theoretical formalism whose power we wish to demonstrate and popularize in this paper.

III. VORTICES AND MEAN FIELD THEORY OF VORTEX INTERACTIONS

A. The classification of topological solutions and the vortex Hamiltonian

Now we discuss the possible topological solitons in our system. Remember once again that they differ from dynamical solitons such as those studied in [12] and references therein. In order to classify the topologically nontrivial solutions, consider first the symmetries of the Lagrangian (4). It describes a doublet of 2D complex fields which interact solely through the phase-invariant total intensity $I = \Psi^\dagger \Psi$ (and the spatial derivative term $|\nabla \Psi|^2$), while in the kinetic term $\Psi^\dagger \sigma_3 \partial_z \Psi$ the two components have opposite signs of the "time" derivative, so this term cannot be reduced to a functional of I . The intensity I has the symmetry group $SU(2)$ (the isometry group of the three-dimensional sphere in Euclidean space) and the kinetic term has the group $SU(1,1)$ (the transformations which leave the combination $|F|^2 - |B|^2$ invariant, i.e. the isometry of the hyperboloid). The intersection of these two is the product $U(1)_F \otimes U(1)_B$: the forward- and backward-propagating doublet (F, B) has phases $\theta_{F,B}$ which can be transformed independently, as $\theta_{F,B} \mapsto \theta_{F,B} + \delta\theta_{F,B}$.

The classification of possible topological solitons is straightforward from the above discussion [34]. They can be characterized in terms of homotopy groups. To remind, the homotopy group π_n of the group G is the group of transformations which map the group manifold of G onto the n -dimensional sphere \mathbb{S}_n . In D -dimensional space the group π_{D-1} therefore classifies what a field configuration looks like from far away (from infinity): it classifies the mappings from the manifold of the internal symmetry group of the system to the spherical "boundary shell" in physical space at infinity. Since the beams in our PR crystal effectively see a two-dimensional space (we regard z as time), we need the first homotopy group π_1 to classify the topological solitons. Since $\pi_1(U(1)) = \pi_1(\mathbb{S}_1) = \mathbb{Z}$ and $\pi_1(\mathbb{G} \otimes \mathbb{G}) = \pi_1(\mathbb{G}) \otimes \pi_1(\mathbb{G})$ for any group \mathbb{G} , the topological solutions are flavored vortices, and the topological charge is the pair of integers $\{Q_F, Q_B\}$.

Let us now derive the effective interaction Hamiltonian for the vortices and study the phase diagram – first in the mean field picture, and then the RG flow for a zoom-in about the critical points and lines. In principle, this story is well known: for a vortex at \mathbf{r}_0 , in the polar coordinates (r, ϕ) , we write $\Psi(\mathbf{r}) = \psi \exp(i\theta(\mathbf{r}))$ for $|\mathbf{r} - \mathbf{r}_0|/|\mathbf{r}_0| \ll 1$, and a vortex of charge Q has $\theta(\phi) = Q\phi/2\pi$. In general the phase has a regular and a singular part, $\nabla \Psi = \psi(\nabla \theta^{(0)} + \nabla \times \zeta \mathbf{e}_z)$, where finally $\zeta = Q \log |\mathbf{r} - \mathbf{r}_0|$. The difference in the PR beam system lies in the existence of two beam fields (flavors) and the non-constant amplitude field $\psi_\pm(r)$, so the vortex looks like

$$\Psi_\pm(\mathbf{r}) = \psi_\pm(r) e^{i\theta_{0\pm}(\phi) + i\theta_\pm(\phi)}. \quad (6)$$

Now the task is to separate the kinetic term of the vortex phase (with $\theta_\pm = \sum_i Q_\pm \log |\mathbf{r} - \mathbf{r}_i|$) from (i) the intensity fluctuations $\delta\psi_\pm$ about some background value $\psi_{0\pm}$ and (ii) the non-vortex phase fluctuations $(\theta_{0\pm})$ in (6). To that

end we need the second-order expansion given in the Appendix (Eq. A2). Upon inserting (6) into (A2), one gets a quadratic action for $\delta\psi_{\pm}$ which is linearly coupled to the phase:

$$\mathcal{L} = \frac{1}{2} (\psi_+'^2 + \psi_-'^2) + \frac{\psi_{\alpha}^2}{2r^2} |\nabla\theta_{\alpha}|^2 + \delta\psi_{\alpha} \hat{K}^{\alpha\beta} \delta\psi_{\beta} + (\delta\psi_{\alpha}^{\dagger} \psi_{0\alpha} \nabla\theta_{0\alpha} \nabla\theta_{\alpha} + \text{h.c.}) + \dots, \quad (7)$$

where (...) denote all terms of cubic or higher order in amplitude as well as the terms which only depend on the regular (non-winding) phase $\theta_{0\alpha}$. Primes denote the derivatives with respect to r . The matrix \hat{K} contains complicated combinations of Γ, I_0, I_x, τ , determined by the potential (5) and its expansion (A2). Now we integrate out the amplitude fluctuations and end up with same-flavor coupling between the winding phase which is already present in the very first term in (7), *and* the coupling between the vortices of different flavors, which comes from the last term in (7) upon integrating out $\delta\psi_{\alpha}$. Now to package the vortex-vortex interaction in the Coulomb-like form is a textbook calculation trivially generalized for the two-flavor field, giving the Lagrangian for N vortices at locations $\mathbf{r}_i, i = 1, \dots, N$ with charges $\{Q_{i+}, Q_{i-}\}$. From this point on it is more convenient to look at the vortex Hamiltonian $\mathcal{H}_{\text{vort}}$ – the difference from the Lagrangian lies just in the sign of the term V_{eff} . The value of \mathcal{H} on a given configuration is the formal energy; the states with lower energy will be preferable. In order to write the Hamiltonian (and further manipulations with it) in a concise way, it is handy to introduce shorthand notation $\vec{Q} \equiv (Q_+, Q_-)$, $\vec{Q}_1 \cdot \vec{Q}_2 \equiv Q_{1+}Q_{2+} + Q_{1-}Q_{2-}$, and $\vec{Q}_1 \times \vec{Q}_2 \equiv Q_{1+}Q_{2-} - Q_{1-}Q_{2+}$. For the self-interaction within a vortex \vec{Q}_1 , we have $\vec{Q}_1 \cdot \vec{Q}_1 = Q_{1+}^2 + Q_{1-}^2$ but $\vec{Q}_1 \times \vec{Q}_1 \equiv Q_{1+}Q_{1-}$ (i.e. there is a factor of 2 mismatch with the case of two different vortices). Now the Hamiltonian reads

$$\mathcal{H}_{\text{vort}} = \sum_{i < j} \left(g \vec{Q}_i \cdot \vec{Q}_j + g' \vec{Q}_i \times \vec{Q}_j \right) \log r_{ij} + \sum_i \left(g_0 \vec{Q}_i \cdot \vec{Q}_i + g_1 \vec{Q}_i \times \vec{Q}_i \right), \quad (8)$$

with $r_{ij} \equiv |\mathbf{r}_i - \mathbf{r}_j|$, and the indices $1 \leq i, j \leq N$ sum over all the vortices. The coupling constants g, g', g_0, g_1 are the result of integrating out the intensity fluctuations and in general are given by rather cumbersome (and not very illustrative) functions of Γ, I_0, τ . We give the expressions at leading order just for comparison with numerics:

$$\begin{aligned} g &= I_0 + \frac{4b + 2I_0}{(2b + 3I_0)(2b - I_0)} \\ g' &= \frac{4I_0}{(2b + 3I_0)(2b - I_0)} \\ b &= \Gamma \frac{1 + \frac{\tau}{L} - \tau \frac{I_0 + I_x}{1 + I_0 + I_x}}{2 \left(1 + \frac{\tau}{L} - \tau \frac{I_0 + I_x}{1 + I_0 + I_x} \right)^2} \left(2 + 2\frac{\tau}{L} + 2I_x + 3I_0 \right). \end{aligned} \quad (9)$$

The meaning of the Hamiltonian (8) is obvious. The first term is the Coulomb interaction of vortices; notice that only like-flavored charges interact through this term (because the kinetic term $|\nabla\Psi|^2$ is homogenous quadratic). The second term is the forward-backward interaction, also with Coulomb-like (logarithmic) radial dependence. This interaction comes from the mixing of the F - and B -modes in the term in brackets in Eq. (7), and is generated, as we commented above, when the amplitude fluctuations $\delta\psi_{\alpha}(r)$ are integrated out. The third and fourth term constitute the energy of the vortex core. The self-interaction constants g_0, g_1 are of course dependent on the vortex core size and behave roughly as $g \log a/\epsilon, g' \log a/\epsilon$, where ϵ is the UV cutoff. The final results will not depend on ϵ , as expected, since g_0, g_1 can be absorbed in the fugacity y (see the next subsection).

Overall, the Hamiltonian (8) is a straightforward two-flavor generalization of the vortices in the XY model. In three space dimensions, vortices necessitate the introduction of a gauge field [14] which, in multi-component systems, also acquires the additional flavor index [19, 21]. In our case, there is no emergent gauge field and the whole calculation is a rather basic exercise at the textbook level but the results are still interesting in the context of nonlinear optics and analogies to magnetic systems: they imply that the *phase* structure (vortex dynamics) can be spotted by looking at the *intensity* patterns (light intensity I or local magnetization \mathcal{M} , see the penultimate section).

B. The phase diagram

1. The mean-field theory for vortices

The phases of the system can be classified at the mean field level, following e.g. [14, 36]. One may look at the free energy of a single vortex (Q_+, Q_-) , which equals $\mathcal{F}_1 = \mathcal{H}_1 - (1/L)S_1$. Here one should remember that inverse

thermodynamic temperature β is identified with the inverse length $1/L$, since L is the radius of compactification of the z -axis, so we can use the usual thermodynamic relation between the free energy \mathcal{F} and (internal) energy \mathcal{H} . The entropy is given by the number of ways to place a vortex of core size a in the plane of size $\Lambda \gg a$: $S \sim \log(\Lambda/a)^2$. Suppose for now that elementary excitations have $|Q_{\pm}| \leq 1$, as higher values increase the energy but not the entropy. Now we can consider the case of single-charge vortices with possible charges $(1, 0)$, $(-1, 0)$, $(0, 1)$, $(0, -1)$, and the case of two-charge vortices where F - and B -charge may be of the same sign or of the opposite sign, $(1, 1)$, $(-1, -1)$, $(1, -1)$, $(-1, 1)$:

$$\mathcal{F}_0 = \left(g - \frac{2}{L}\right) \log \frac{\Lambda}{a}, \quad \vec{Q} = (\pm 1, 0) \text{ or } \vec{Q} = (0, \pm 1) \quad (10)$$

$$\mathcal{F}_1 = \left(2g - 2g' - \frac{2}{L}\right) \log \frac{\Lambda}{a}, \quad (Q_+, Q_-) = (\pm 1, \mp 1) \quad (11)$$

$$\mathcal{F}_2 = \left(2g + 2g' - \frac{2}{L}\right) \log \frac{\Lambda}{a}, \quad (Q_+, Q_-) = (\pm 1, \pm 1). \quad (12)$$

Now we identify four regimes, assuming that $g, g' > 0$ [49]:

1. For $L > 2/g$ a vortex always has positive free energy so vortices are unstable like in the low-temperature phase of the textbook BKT system. This is the vortex-free phase where the phase $U(1)_F \otimes U(1)_B$ does not wind. This phase we logically call *vortex insulator* in analogy with the single-flavor case.
2. For $2/g > L > 1/(g - g')$ a double-flavor vortex always has positive free energy but single-flavor vortices are stable; in other words, there is proliferation of vortices of the form $\vec{Q} = (Q_+, 0)$ or $\vec{Q} = (0, Q_-)$. This phase is like the conductor phase in a single-component XY model, and the topological excitations exist for the reduced symmetry group, i.e. for a single $U(1)$. We thus call it *vortex conductor*; it is populated mainly by single-flavor vortices $(Q, 0)$, $(0, Q)$.
3. For $1/(g - g') > L > 1/(g + g')$ double-vortex formation is only optimal if the vortex has $Q_+ + Q_- = 0$ which corresponds to the topological excitations of the diagonal $U(1)_d$ symmetry subgroup, the reduction of the total phase symmetry to the special case $(\theta_F, \theta_B) \mapsto (\theta_F + \delta\theta, \theta_B - \delta\theta)$. In other words, vortices of the form $(Q_+, -Q_+)$ proliferate. Here higher charge vortices may be more energetically favorable than unit-charge ones, contrary to the initial simplistic assumption, the reason being that the vortex core energy proportional to gQ_+^2 may be more than balanced out by the intra-vortex interaction proportional to $-g'Q_+^2$ (depending on the ratio of g and g'). This further means that there may be multiple ground states of equal energy (frustration). We thus call this case *frustrated vortex insulator* (FI); it is populated primarily with vortices of charge $(Q, -Q)$.
4. For $1/(g + g') > L$ vortex formation always reduces the free energy, no matter what the relation between Q_+ and Q_- is, and each phase can wind separately: $(\theta_F, \theta_B) \mapsto (\theta_F + \delta\theta_F, \theta_B + \delta\theta_B)$. Vortices of both flavors proliferate freely at no energy cost and for that reason we call this phase *vortex perfect conductor* (PC). We deliberately avoid the term superconductor to avoid the (wrong) association of this phase with the Abrikosov vortex lines and type I/type II superconductors familiar from the 3D vortex systems: remember there is no emergent gauge field for the vortices in two spatial dimensions, and we only have perfect conductivity in the sense of zero resistance for transporting the (topological) charge, but no superconductivity in the sense of breaking a gauge symmetry.

A more systematic mean-field calculation will give the phase diagram also at zero temperature, i.e. the "quantum" phase transitions at large L . Starting from the Hamiltonian (8), we introduce the order parameter fields in the following way. Denote the number of vortices with charge $(1, 1)$ by ρ_{2+} and the number of vortices $(1, -1)$ by ρ_{2-} ; due to charge conservation, this means we also have ρ_{2+} vortices of type $(-1, -1)$ and ρ_{2-} vortices with charge $(-1, 1)$. The number of single-charge vortices of type $(1, 0)$ and $(0, 1)$ is denoted by ρ_{1+} and ρ_{1-} , respectively. Denote also $\rho_2 \equiv \rho_{2+} + \rho_{2-}$ and $\delta\rho_2 \equiv \rho_{2+} - \rho_{2-}$ (notice that $-\rho_2 \leq \delta\rho_2 \leq \rho_2$), and finally $\rho_1 \equiv \rho_{1+} + \rho_{1-}$. We insert this into the vortex Hamiltonian $\mathcal{H}_{\text{vort}}$, and assume that the long-ranged logarithmic interaction $\log r_{ij}$ justifies the mean-field approximation: for $i \neq j$ we can approximate $\log r_{ij} \sim \log \Lambda$, assuming that average inter-vortex distance is of the same order of magnitude as the system size. For the core energy, we know that $g_0, g_1 \sim \log(a/\epsilon) \sim -\log \epsilon \sim \log \Lambda$, where in the last equality we have assumed that the UV cutoff ϵ is of similar order of magnitude as the inverse of the IR cutoff $1/\Lambda$, which is natural [50]. Thus all terms are proportional to $\log \Lambda$ and we can write

$$\mathcal{F}_{\text{mf}} = \beta \log \frac{\Lambda}{a} [2(g - 1)\rho_2 + 2g'\delta\rho_2 + (g - 1)\rho_1] \equiv A\rho_2 + B\delta\rho_2 + \frac{B}{2}\rho_1 \quad (13)$$

Now the ground state is determined by minimizing the free energy, i.e. the effective action of the system. Notice that \mathcal{F}_{mf} is linear in the fields $\rho_2, \delta\rho_2, \rho_1$ so the optimal configurations have either $\mathcal{F}_{\text{mf}} = 0$ or $\mathcal{F}_{\text{mf}} \rightarrow -\infty$, and the

mean-field densities $\rho_{1,2}$ are either zero, or arbitrary (formally infinite). This is a well-known property of the 2D Coulomb gas and has to do with the fact that (assuming the cutoff dependence has been eliminated) this system is conformal invariant in the insulator phase, so all finite densities ρ are equivalent: there is no other scale to compare ρ to. Likewise, the inverse "temperature" β can be absorbed into the definition of the coupling constants g, g' and thus is not an independent parameter (this is well-known also from the single-flavor case). Minimizing (13) is an elementary exercise and we find again four regimes, corresponding to the four phases we guessed above:

1. For $A > 0, A > |B|$ the minimum is reached for $\rho_2 = \delta\rho_2 = \rho_1 = 0$. In the ground state there are no vortices at all – the system is a vortex insulator.
2. For $B > 0, A + B < 0$, giving $g + g' < 1, g' > 0$, the free energy has its minimum for $\rho_2 > 0$ and $\delta\rho_2 = -\rho_2$ (notice that $-\rho_2 \leq \delta\rho_2 \leq \rho_2$). This means $\rho_{2+} = 0, \rho_{2-} > 0$, so opposite-charged vortices $(Q, -Q)$ proliferate, and the system is dominated by the interactions between the charges. This is the frustrated vortex insulator regime. Since $g' < 0$, the single-charge vortices (density ρ_1) are suppressed.
3. For $B < 0, A + B < 0$, i.e. $g + g' < 1, g' < 0$ the minimum is reached for $\rho_2 = \delta\rho_2 > 0$, i.e. $\rho_{2-} = 0$ so the vortices (Q, Q) can proliferate. However, since $g' < 0$ there is also nonzero single-flavor density ρ_1 and the proliferation of vortices $(Q, 0)$ and $(0, Q)$ which generically dominate over two-flavor vortices. This is the conductor phase, with mostly single-flavor vortices (as in the standard XY model).
4. The point $A = B = 0$ is special: naively, from (13) arbitrary nonzero $\rho_1, \rho_2, \delta\rho_2$ are allowed. Of course, higher-order corrections will change this but the energy cost of vortex formation will generically be smaller than in previous phases. This is the vortex perfect conductor phase. In the mean-field approach it looks like a single point, but that will turn out to be an artifact of the mean-field approach: for small nonzero A, B the system still remains in this phase.

In terms of the original parameters g, g' , one sees the insulator phase is given by $g + g' > 1$, and the conductor and the FI are separated by the line $g' = 0$. We can now sketch the phase diagram, which is given in Fig. 2(A), side by side with the refinement obtained by the RG flow, in the next subsection. Of course, all of this is an elementary problem in statistical mechanics but it has some interesting consequences as we will see.

2. RG analysis

We have classified the symmetries and thus the phases of our system at the mean-field level. To describe quantitatively the borders between the phases and the phase diagram, we will perform the renormalization group (RG) analysis. Here we follow closely the calculation for conventional vortex systems [14]. We consider the fluctuation of the partition function $\delta\mathcal{Z}$ upon the formation of a virtual vortex pair at positions $\mathbf{r}_1, \mathbf{r}_2$ with charges $\vec{q}, -\vec{q}$, (with $\mathbf{r}_1 + \mathbf{r}_2 = 2\mathbf{r}$ and $\mathbf{r}_1 - \mathbf{r}_2 = \mathbf{r}_{12}$), in the background of a vortex pair at positions $\mathbf{R}_1, \mathbf{R}_2$ (with $\mathbf{R}_1 + \mathbf{R}_2 = 2\mathbf{R}$ and $\mathbf{R}_1 - \mathbf{R}_2 = \mathbf{R}_{12}$) with charges \vec{Q}_1, \vec{Q}_2 . This is a straightforward but lengthy calculation and we state just the main steps. First, it is easy to show that the creation of single-charge vortices is irrelevant for the RG flow so we disregard it. Also, we can replace the core self-interaction constants $g_{0,1}$ with the fugacity parameter defined as $y \equiv \exp(-(\beta g_0 + \beta g_1) \log \epsilon)$.

Now from the vortex Hamiltonian $\mathcal{H}_{\text{vort}}$ the fluctuation equals (at the quadratic order in y and r):

$$\frac{\delta\mathcal{Z}}{\mathcal{Z}} = 1 + \frac{y^4}{4} \sum_{q_{\pm}} \int dr_{12} r_{12}^3 e^{g\vec{q} \cdot \vec{q} + g'\vec{q} \times \vec{q}} \left[\int dr r^2 \left(g\vec{Q}_1 \cdot \vec{q} + g'\vec{Q}_1 \times \vec{q} \right) \nabla \log |\mathbf{R}_1 - \mathbf{r}| + \left(g\vec{Q}_2 \cdot \vec{q} + g'\vec{Q}_2 \times \vec{q} \right) \nabla \log |\mathbf{R}_2 - \mathbf{r}| \right]^2. \quad (14)$$

Notice that ∇ is taken with respect to \mathbf{r} . The above result is obtained by expanding the Coulomb potential in r_{12} (the separation between the virtual vortices being small because of their mutual interaction) and then expanding the whole partition function (i.e. the exponent in it) in y around the equilibrium value \mathcal{Z} . The term depending on the separation r_{12} is the mutual interaction energy of the virtual charges, and the subsequent term proportional to r^2 is the interaction of the virtual vortices with the external ones (the term linear in r cancels out due to isotropy). Then by partial integration and summation over $q_{\pm} \in \{1, -1\}$ we find

$$\begin{aligned} \frac{\delta\mathcal{Z}}{\mathcal{Z}} = 1 + y^4 & \left(8\pi g^2 \vec{Q}_1 \cdot \vec{Q}_2 + 8\pi (g')^2 \vec{Q}_1 \cdot \vec{Q}_2 + 16\pi g g' \vec{Q}_1 \times \vec{Q}_2 \right) I_3 \log R_{12} + \\ & + y^4 \left(4\pi g (g + g') \left(\vec{Q}_1 \times \vec{Q}_1 + \vec{Q}_2 \times \vec{Q}_2 \right) I_1 + 8(g')^2 I_1 \right) \log \epsilon, \end{aligned} \quad (15)$$

with $I_n = \int_a^{\Lambda a} dr r^{n+g+g'}$, and all integrals are in the limits from ϵa to Λa . Now taking into account the definition of the fugacity y , rescaling $\Lambda \mapsto \Lambda(1+\ell)$, performing the spatial integrals and expanding over ℓ , we can equate the bare quantities g, g', y in (8) with their corrected values in $\mathcal{Z} + \delta\mathcal{Z}$ to obtain the RG flow equations:

$$\begin{aligned}\frac{\partial g}{\partial \ell} &= -16\pi(g^2 + g'^2)y^4 \\ \frac{\partial g'}{\partial \ell} &= -2\pi g g' y^4 \\ \frac{\partial y}{\partial \ell} &= 2\pi(1 - g - g')y.\end{aligned}\tag{16}$$

Now let us consider the fixed points of the flow equations. If one puts $g' = 0$, they look very much like the textbook XY model RG flow, except that the fugacity enters as y^4 instead of y^2 (since the energy of the vortex core now has two contributions, from g - and g' -interactions). They yield the same phases as the mean-field approach as it has to be, but now we can numerically integrate the flow equations to find exact phase borders. The fugacity y can flow to zero (meaning that the vortex creation is suppressed and the vortices tend to bind) or to infinity, meaning that vortices can exist at finite density. At $y = 0$ there is a fixed line $g + g' = 1$. This line is attracting for the half-plane $g + g' > 1$; otherwise, it is repelling. There are three more attraction regions when $g + g' < 1$. First, there is the point $y \rightarrow \infty, g = g' = 0$ which has no analogue in single-component vortex systems. Then, there are two regions when $g \rightarrow \infty$ and $g' \rightarrow \pm\infty$ (and again $y \rightarrow \infty$). Of course, these are the strongly interacting phases when the perturbation theory breaks down, so in reality the coupling constants grow to some finite values g_*, g'_* and g_{**}, g'_{**} rather than to infinities. The situation is now the following:

1. The attraction region of the fixed line is the vortex insulator phase: the creation rate of the vortices is suppressed to zero.
2. The zero-coupling fixed point attracts the trajectories in the vortex perfect conductor phase: only the fugacity controls the vortices and arbitrary charge configurations can form. Here we see it has a finite extent in the parameter space.
3. The attraction region in which $g_* < 0$ while $g'_* > 0$ has like F -charges and B -charges attract each other and the opposite ones repel each other. This is the frustrated insulator.
4. The fixed point with $g_{**}, g'_{**} < 0$ corresponds to the conductor phase.

The RG flows in the $g - g'$ plane are given in Fig. 2(B). In the half-plane $g + g' > 1$ every point evolves toward a different, finite point (g, g') in the same half-plane. In the other half-plane we see the regions of points moving toward the origin or toward one of the two directions at infinity. The PC phase (the attraction region of the point $(0, 0)$) could not be obtained from the mean field calculation (i.e. it corresponds to the single point at the origin at the mean field level).

One may worry that the coupling constants can be negative, with like charges repelling and opposite charges attracting each other. However, this is perfectly allowed in our system. In the usual XY model, the stiffness is proportional to the kinetic energy coefficient and thus has to be positive. Here, the coupling between the fluctuations of F - and B -beams introduces other contributions to g, g' and the resulting expressions (9) give bare values of g, g' that can be negative, and the stability analysis of the RG flow clearly shows that for nonzero g' , the flow can go toward negative values even if starting from a positive value in some parameter range. If we fix $g' = 0$, the flow equations reproduce the ones from the single-component XY model, and the phase diagram is reduced to just the $g' = 0$ line. If we additionally suppose that the bare value of g is non-negative, then we are on the positive $g' = 0$ semiaxis in the phase diagram – here we see only two phases, insulator (no vortices, $g \rightarrow \text{const.}$) and perfect conductor ($g \rightarrow 0$). However, or g' fixed to zero (that is, with a single flavor only), the perfect conductor reduces to the usual conductor phase of the single-component XY model – in other words, we reproduce the expected behavior.

Physically, it is preferable to give the phase diagram in terms of the quantities Γ, τ, I_0, I_x that appear in the initial equations of motion (1-2): the light intensities can be directly measured and controlled, whereas the relaxation time and the coupling cannot, but at least they have a clear physical interpretation. The relations between these and the effective Hamiltonian quantities y, g, g' are found upon integrating out the intensity fluctuations to obtain (8) and the explicit relations are stated in (9). Making use of these we can also plot the phase diagram in terms of the physical quantities. We nevertheless retain one emergent parameter, g' , and plot the $\Gamma - g'$ phase diagram in Fig. 3. The non-interacting fixed point $g = g' = 0$ is now mapped to $\Gamma = 0$. The tricritical point where the PC, the FI and the conductor phases meet is at $R = 1$. Therefore, the rule of thumb is that low couplings Γ produce stable vortices with conserved charges – the perfect vortex conductor. Increasing the coupling pumps the instability up, and the kind of

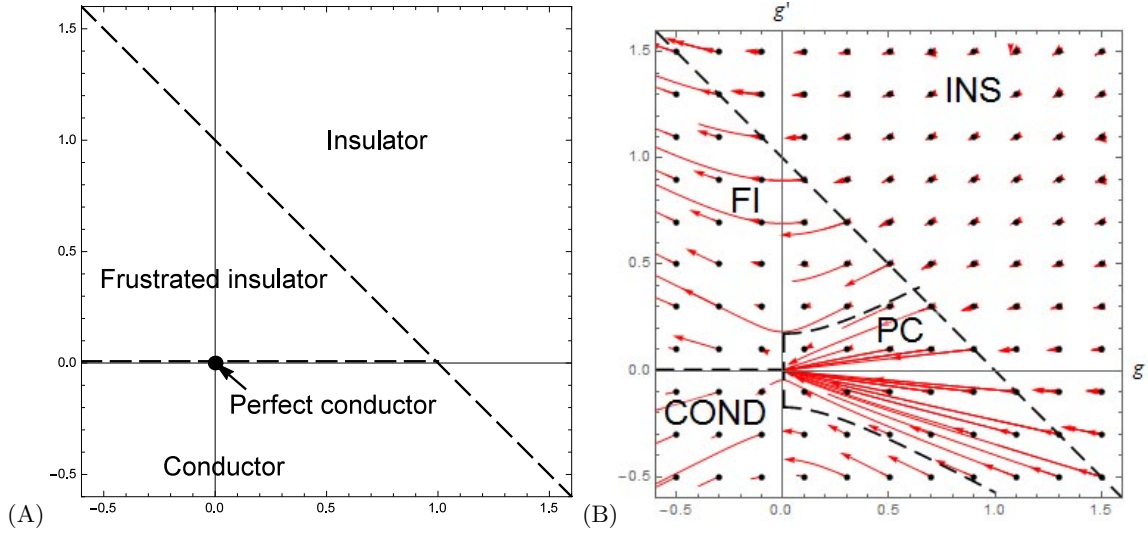


FIG. 2: Phase diagram for the clean system in the g - g' plane, at the mean-field level (A) and with RG flows (red) starting at the black points (B). Four phases exist, whose boundaries are delineated by black dashed lines. In the mean-field calculation (A) all phase boundaries are analytical. In the RG calculation, the straight line $g + g' = 1$ is obtained analytically whereas the other phase boundaries can only be found by numerical integration of the flow equations (16). The flows going to infinity are the artifacts of the perturbative RG; they probably correspond to finite values which are beyond the scope of our analytical approach. We show the flows for a grid of initial points, denoted by black dots; red lines are the flows. Notice how the flows in the $g + g' > 1$ phase all terminate at different values.

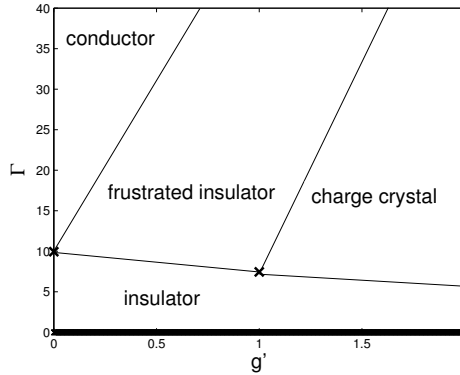


FIG. 3: Phase diagram in the clean system, in the Γ - g' plane. There are two discrete fixed points and the critical line at $\Gamma = 0$, which corresponds to the critical line $g + g' = 1$ in the previous figure. We also see two discrete fixed points, corresponding to $g_{*,**}, g'_{*,**}$. The advantage of physical parameters is that the location of these fixed points in the Γ - I plane can be calculated directly from the numerics (or measured from the experiment).

instability (and the resulting phase) is determined by the relative strength of the photonic lattice compared to the propagating beams. Obviously, such considerations are only a rule of thumb and detailed structure of the diagram is more complex. This is one of the main motives of this study – blind numerical search for patterns without the field-theoretical approach adopted here would require many runs for a good understanding of different phases.

C. Geometry of patterns

Now we discuss what the intensity pattern $I(\mathbf{r})$ looks like in various phases, for various boundary conditions. This is very important as this is the only thing which can be easily measured in experiment – phases are not directly observable, while the intensity distribution is the direct outcome of the imaging of the crystal [23]. We shall consider three situations. The first is a single Gaussian beam on zero background ($I_x = 0$), with Gaussian initial intensity profile $|F(z = 0, \mathbf{r})|^2 = |B(z = L, \mathbf{r})|^2 = \mathcal{N} \exp(-r^2/2\sigma^2)$ and possibly non-zero vortex charges:

$\arg \Psi_{\pm}(\mathbf{r}) \sim \exp(Q_{F,B}\phi)$, with $\mathbf{r} = (r \cos \phi, r \sin \phi)$. This is relevant to check the basic mechanism of the topological protection of the vortices and to study the forward-backward coupling g' . The second is again the Gaussian beam but now on a background square photonic lattice of spacing a . Each lattice site is again a Gaussian beam, so the total background intensity is of the form $I_x = \sum_{i,j} \exp\left(-(x-x_i)^2/2\sigma^2 - (y-y_i)^2/2\sigma^2\right)$, where $x_{i+1} - x_i = y_{i+1} - y_i = a$. Here we can consider the vortex pinning to defects and the creation/annihilation processes with vortices. The third case is a quadratic vortex lattice of F - and B -beams with lattice spacing a (giving now for the beam intensity $I_0 = \sum_{i,j} \exp\left(-(x-x_i)^2/2\sigma^2 - (y-y_i)^2/2\sigma^2\right)$), the situation particularly relevant for analogies with condensed matter systems. In this case we usually also turn on the background photonic lattice, which is either coincident or off-phase (shifted for half a lattice spacing $a/2$) with the beam lattice.

First of all, it is important to notice that there are two kinds of instabilities that can arise in a vortex beam [51]:

- There is an instability which originates in the disbalance between the diffusion and self-focusing (crystal response) in favor of diffusion in *high-gradient regions*: if a pattern $I(x,y)$ has a large gradient ∇I , the kinetic term in the Lagrangian (4), i.e. the diffusion term in (1) is large and the crystal charge response is not fast enough to balance it as we travel along the z -axis, so the intensity rapidly dissipates and the pattern changes. Obviously, the vortex core is a high-gradient region so we expect it to be vulnerable to this kind of instability. This is indeed the case: in the center of the vortex the intensity diminishes, a dark region forms and the intensity moves toward the edges. We dub this the core or central instability (CI), and in the effective theory it can be understood as the decay of states with low fugacity y , i.e. high self-interaction constants g_0, g_1 . This instability prevents the formation of vortices in the insulator phase, or limits it in the frustrated insulator and conductor phases.
- There is an instability stemming from the dominance of diffusion over self-focusing in *low-intensity regions of sufficient size and/or convenient geometry*. At low-intensity, the charge response is nearly proportional to I (from Eq. 2), so if I is small diffusion wins and the intensity dissipates. If there is sufficient inflow of intensity from more strongly illuminated regions, it may eventually balance the diffusion; but if the pattern has a long "boundary", i.e. outer region of low intensity, it will not happen and the pattern will dissipate out, or reshape itself to reduce the low-intensity region. We call this case the edge instability (EI). For a vortex, it happens when the positive and negative vortex charges tend to redistribute due to Coulomb attraction and repulsion. In our field theory Hamiltonian (8), this instability dominates in the conductor and perfect conductor phases.

Qualitative characterization of instabilities is important to recognize different phases and order/disorder phenomena in experiment, as the beam phase θ cannot be measured directly. We first show how the CI and EI work for single beams with nonzero vortex charge. In Fig. 4 we show the intensity patterns for a single vortex with charges (1, 0) and (3, 0) as the $x-y$ cross sections in the middle of the crystal, i.e. for $z = L/2$. The parameters chosen (Γ, I_0, R, L) correspond to the conductor phase (top) and the insulator phase (bottom). In top panels, for $Q_+^2 + Q_-^2 = 1$ the core energy is not so large and CI is almost invisible. For $Q_+^2 + Q_-^2 = 9$ we see the incoherence and the dissipation in the core region, signifying the CI. We see the conductor phase allows the proliferation of vortices but only those with $|Q_{\pm}| \leq 1$ are stable. In the bottom panels, both vortices have almost dissipated away due to EI, which starts from discrete poles near the boundary [52]. Indeed, the insulator phase has no free vortices, no matter what the charge. In Fig. 5 we see no instability even for the multi-quantum vortex in the perfect conductor phase (top), whereas the frustrated insulator phase (bottom) shows strong EI for the opposite-charged vortex (3, -3) since this fixed point has $g'_* > 0$ but the (3, 3) vortex is stable. Notice that we could not expect CI for this case since the sum $Q_+^2 + Q_-^2 = 9$ is the same in both cases – if the $Q_+ = -Q_-$ vortex shows no CI, the same situation with opposite Q_- cannot show it either. We have thus seen what patterns to expect from CI and EI, and also what kind of stable vortices to expect in different phases: *the perfect conductor phase allows free proliferation of vortices of any charge, the conductor phase allows only single-quantum vortices (or vortices with sufficiently low $Q_+^2 + Q_-^2$) while others dissipate from CI, the frustrated insulator supports the vortices with favorable charges (and charge distribution in multiple-vortex systems) while others disintegrate from EI, and the insulator phase supports no vortices – they all dissipate from CI or EI, whichever settles first (depending on the vortex charges).*

The case rich with analogies with condensed matter systems is the square vortex lattice on the background photonic square lattice, Fig. 6. Here we can also appreciate the transport processes. The photonic lattice is coincident with the beam lattice and equal in intensity, so $\Gamma(I_0 + I_x) = 2\Gamma I_0$. In the perfect conductor phase (top left) the vortices are stable and coherent and keep the uniform lattice structure. In the conductor phase (top right) the CI is visible but the lattice structure survives. The bottom panels show the non-conducting phases, insulator (bottom left) and frustrated insulator (bottom right). The former loses both lattice periodicity and the Gaussian profile of the vortices but the latter keeps regular structure: from EI the intensity is *inverted* and the resulting lattice is *dual* to the original one (compare to top left). The phase patterns $\theta_F(x, y; z = L/2)$ and $\theta_F(x, z; y = 320\mu\text{m})$ for the perfect conductor

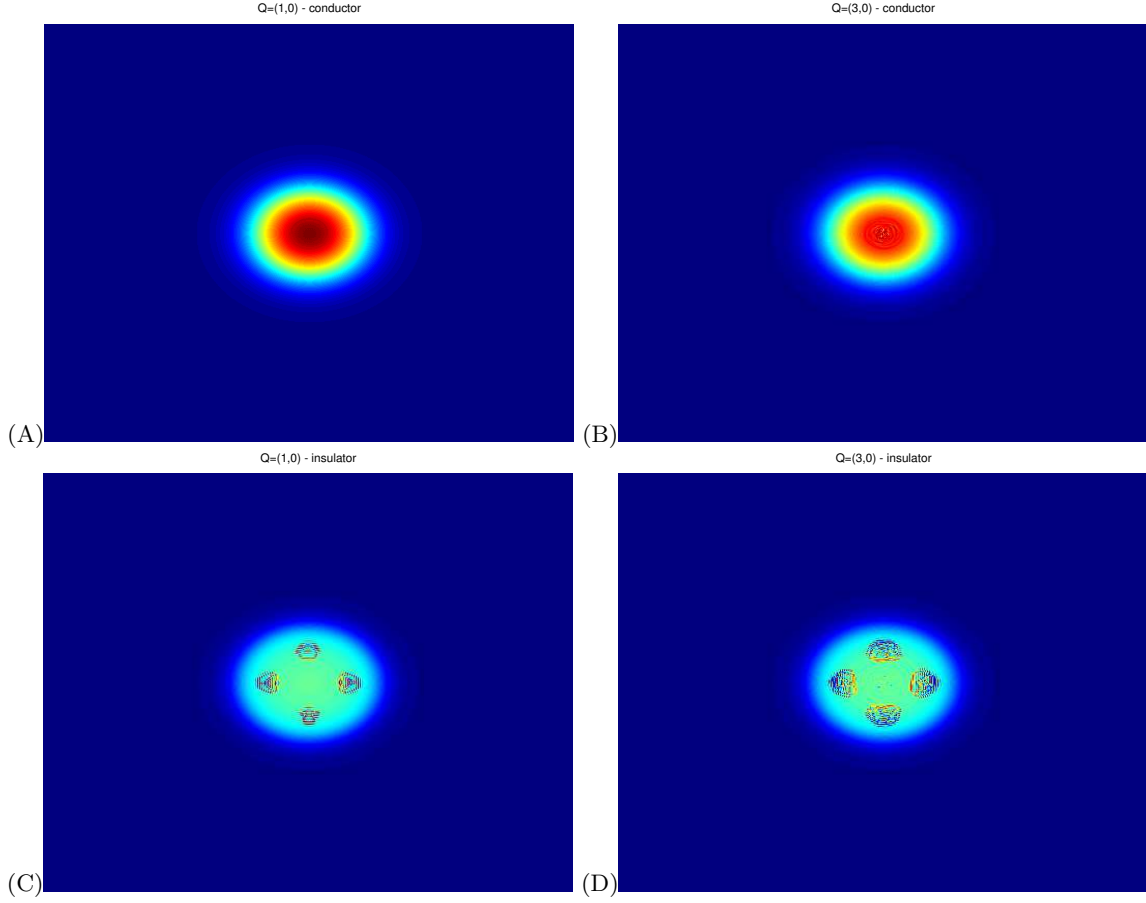


FIG. 4: Two single Gaussian beams (FWHM $40\mu\text{m}$) with vortex charges $(1, 0)$ (A, C) and $(3, 0)$ (B, D), with $\Gamma I_0 = 41$ and $L = 2.4\text{mm}$ (top) and $L = 4.8\text{mm}$ (bottom) at the back face of the crystal ($z = L$). The regime on top (A, B) corresponds to the conductor phase, which has a single (independent) conserved vortex charge $Q_F = -Q_B$. This topological protection prevents significant instabilities; nevertheless, the multi-quantum vortex $(3, 0)$ shows the onset of CI - notice the reduced intensity and incoherent distribution of the beam in the central region in the top right panel (the CI is expected to grow roughly as $Q_+^2 + Q_-^2$). The insulator phase only preserves the $F - B$ invariance but not the vortex charge and in absence of topological protection the vortices can annihilate into the vacuum - here we see the EI taking over for both charges - four unstable regions appear near the boundary, violating the circular symmetry and dissipating away the intensity of the vortex.

(top) and the frustrated insulator phase (bottom) are shown in the Fig. 7. Here we see the vortex charge transport mechanism in a perfect conductor: the vortices are connected in the sense that the phase is coherently traveling from one vortex to the next. In the frustrated insulator phase, the phase is initially frozen along the z -axis, until the transport starts at some $z \approx L/2$.

It may be instructive to take a closer look at the lattice dynamics of the most interesting phase: the frustrated insulator. In Fig. 8 we inspect square lattices on the photonic lattice background for several charges of the form $(Q_+ = 3, Q_-)$. First, we see how the vortices loose stability and develop CI as the total square of the charge grows (from (A) to (C)). Then we notice how the g' coupling favors the opposite sign of Q_+ and Q_- and how the optimal configuration is found for $Q_- = -3$. This is easily seen by minimizing the free energy over Q_- : it leads to the conclusion that the forward-backward coupling favors the "antiferromagnetic" ordering in the sense that $Q_+ + Q_- = 0$. Finally, it is interesting to see how the FI phase and high intensities and coupling strengths contains a seed of translation symmetry breaking which will become important in the presence of disorder. In Figs. 9-10 we give intensity and phase images across the PC-FI transition and deep into the FI phase at large couplings. The intensity maps show the familiar inverse square lattice but more interesting are the phase maps which show stripe-like ordering in Fig. 10(C,D) - horizontal and vertical lines with a repeating constant value of the phase θ_F on all lattice cells along the line. This is a new instability which breaks translation invariance. We cannot easily derive this instability from the perturbation theory in the Appendix as it is a collective phenomenon and not cannot be understood from a single beam or single vortex. We will see in the next section that in the presence of disorder this instability leads to nonzero local charge density.

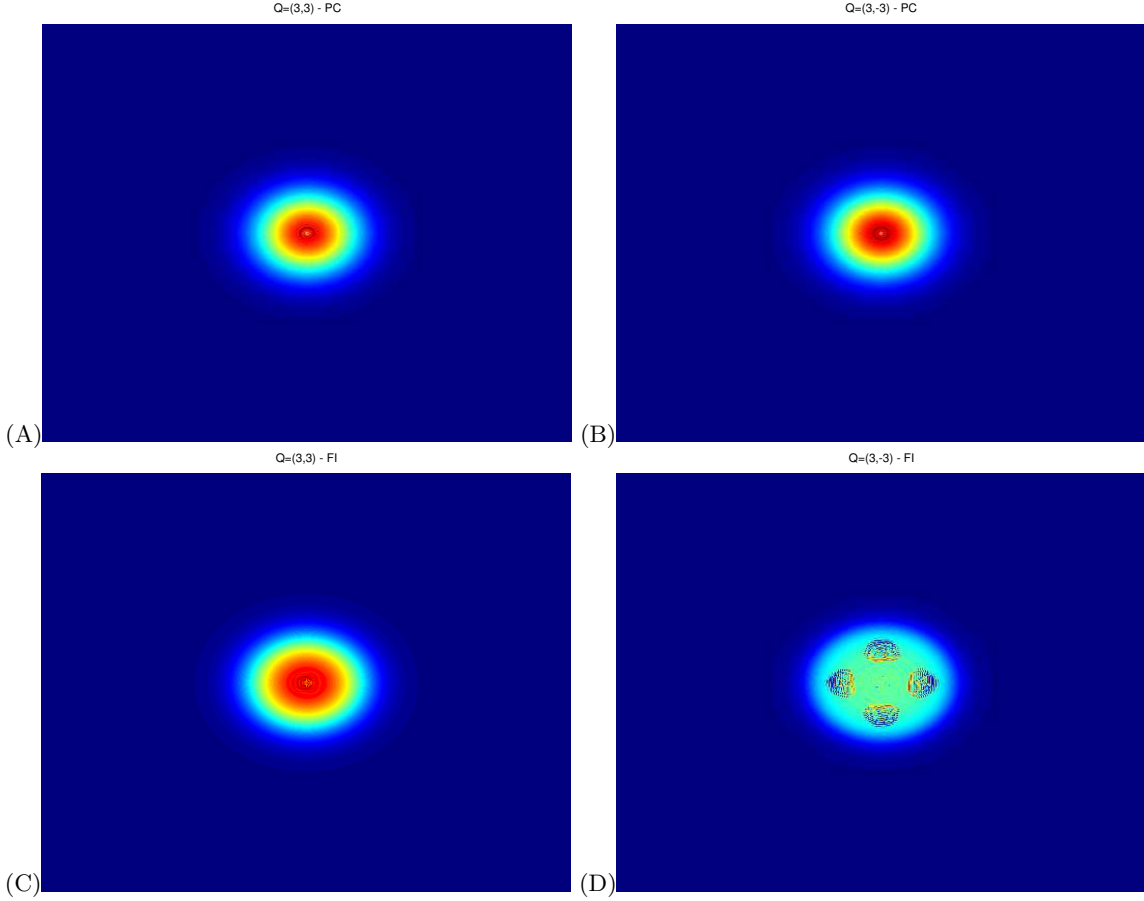


FIG. 5: Two single Gaussian beams with vortex charges $(3, 3)$ (A, C) and $(3, -3)$ (B, D), with $L = 2\text{mm}$ and $\Gamma I_0 = 20$ (top) and $\Gamma I_0 = 40$ (bottom) at the back face of the crystal ($z = L$). The regime on top corresponds to the perfect conductor phase, where the vortices of all charges freely proliferate – both vortices are reasonably stable. The bottom case is in the frustrated insulator phase – the forward-backward coupling makes the $(3, -3)$ vortex unstable from EI while the $(3, 3)$ vortex survives.

IV. THE SYSTEM WITH DISORDER

Consider now the same system in the presence of quenched disorder. This is a physically realistic situation: the disorder corresponds to the holes in the photonic lattice which are caused by the defects in the crystalline lattice. The defects are in fixed positions, i.e. they are quenched, whereas the beam is dynamical and can fluctuate. Now $I_x(\mathbf{r}) \rightarrow I_x(\mathbf{r}) + I_h(\mathbf{r})$, i.e., the quenched random part $I_h(\mathbf{r})$ is superimposed to the regular background (whose intensity is I_x). The disorder is given by some probability distribution, assuming no correlations between defects at different places. As in the disorder-free case, the lattice is static and "hard", i.e., does not backreact due to the presence of the beams. One should however bear in mind that the backreaction of the lattice can sometimes be important as disregarding it violates the conservation of the angular momentum, see [26]. Disregarding the backreaction becomes exact when $I_x + I_h \gg |\Psi|^2$, i.e. when the background irradiation is much stronger than the propagating beams.

To treat the disorder we use the well-known replica formalism [35]. For vortex-free configurations, typical experimental values of the parameters suggest that the influence of disorder is small [23, 25, 27]. However, the influence of disorder becomes dramatic when the vortices are present. This is expected, since holes in the lattice can change the topology of the phase field θ_{\pm} (the phase now must wind around the holes). Our equations of motion are still given by the Lagrangian (4), but with $I_x \mapsto I_x + I_h$. In our analytical calculations, we assume that a defect in the photonic lattice changes the lattice intensity from I_x to $I_x + I_h$, with Gaussian distribution of I_h , which translates to the approximately Gaussian distribution of the couplings g, g', g_0, g_1 . In the numerics however, we do a further simplification and model the defects in a discrete way, i.e. at a given spot either there is a lattice cell of intensity I_1 (with probability h), or there isn't (the intensity is zero, with probability $1 - h$). This corresponds to $I_x = I_1/2, I_h = \pm I_1/2$ so the disorder is discrete. Due to the central limit theorem, we expect that the Gaussian analytics should be applicable to our numerics.

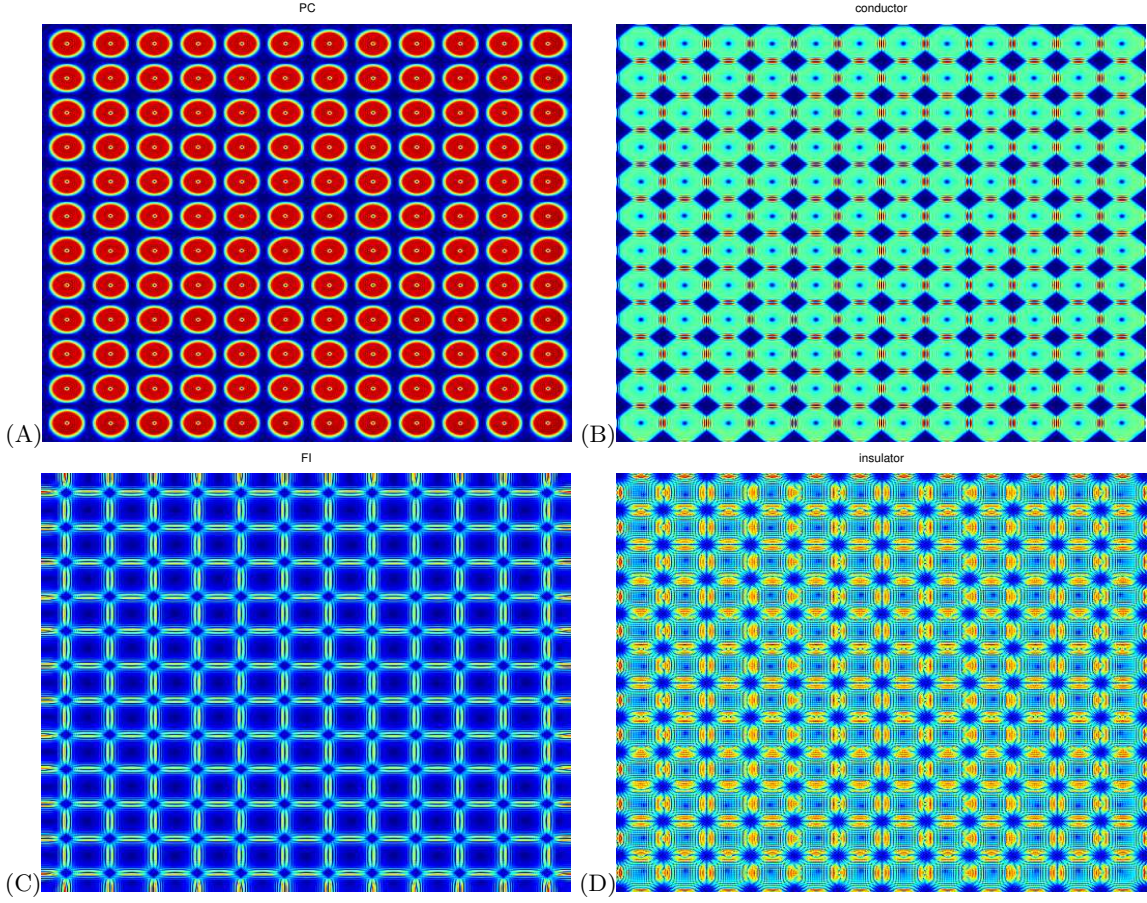


FIG. 6: Vortex lattice with Gaussian profile with FWHM $10\mu\text{m}$ and lattice spacing equal to FWHM, for $\Gamma I = 5$ (PC, panel A), $\Gamma I = 15$ (conductor, panel B), $\Gamma I = 20$ (FI, panel C), and $\Gamma I = 60$ (insulator, panel D); in all cases $L = 4.8\text{mm}$. The perfect conducting phase has a coherent vortex lattice and no instabilities. Conductor exhibits a deformation of the vortex lattice and reduction of the full $O(2)$ symmetry, starting from the *center*, whereas the FI exhibits the reduction of symmetry and inversion of the lattice due to *edge* effects. Notice how both phases have reduced symmetry compared to PC but retain the coherence. Only the insulator phase loses not only symmetry but also coherence, i.e. the intensity diffuses and the pattern is smeared out.

A. The replica formalism at the mean-field level

To study the system with quenched disorder in the photonic lattice, we need to perform the replica calculation of the free energy of the vortex Hamiltonian (8). We refer the reader to the literature [36, 37] for an in-depth explanation of the replica trick. In short, one needs to average over the various realizations of the disorder *prior* to calculating the partition function, i.e. prior to averaging over the dynamical degrees of freedom (vortices in our case). This means that we need to perform the disorder-average of the free energy, i.e. the logarithm of the original partition function $-\log \mathcal{Z}$, and not the partition function \mathcal{Z} itself. The final twist is the identity $\log \mathcal{Z} = \lim_{n \rightarrow 0} (\mathcal{Z}^n - 1)/n$: we study the Hamiltonian consisting of n copies (replicas) of the original system and then *carefully* take the $n \rightarrow 0$ limit. The partition function of the replicated Hamiltonian reads

$$\mathcal{Z} = \lim_{n \rightarrow 0} \text{Tr} \exp \left(- \sum_{\mu=1}^n \mathcal{H}_{\text{vort}} \left(Q^{(\mu)} \right) \right), \quad (17)$$

where $Q^{(\mu)}$ are the vortex charges in the μ -th replica of the system. In the original Hamiltonian (8), the disorder turns the interaction constants into quenched random quantities $g_{ij}, g'_{ij}, g_{0;ij}, g_{1;ij}$, so we can compactly write our interaction term as

$$\mathcal{H}_{\text{vort}} = \sum_{ij} \sum_{\alpha\beta} Q_{i\alpha} J_{ij}^{\alpha\beta} Q_{j\beta} \quad (18)$$

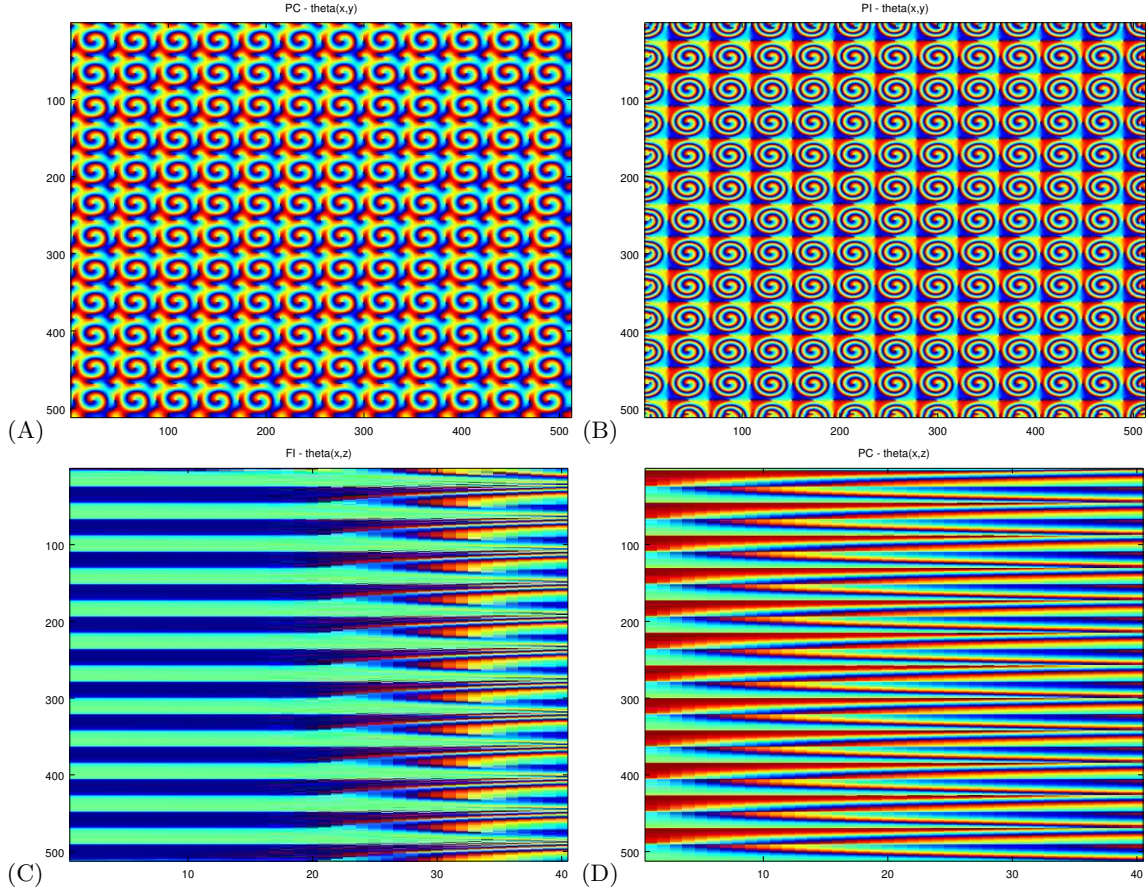


FIG. 7: The (A) and (D) panel from the previous figure (PC and FI) but now we plot the phase θ_F , as the transverse cross-section $\theta_F(x, y; z = L/2)$ (A, B) and as the longitudinal section along the PR crystal $\theta(x, z; y = 320 \mu\text{m})$ (C, D). The perfect conductor phase has well-defined vortices in contact which allows the transport of the vortex charge through the lattice, and shows as the periodical modulation of the phase along the z -axis (vortex lines). The frustrated insulator keeps well-defined vorticity even though the intensity map undergoes inversion (Fig. 6, bottom right) with frozen phase along the z -axis, so there is no vorticity transport until some $z \approx L/2 = 2.4 \text{mm}$, when the phase stripes develop into vortex lines.

with $J_{ij}^{++} = J_{ij}^{--} = g_{ij}(1 - \delta_{ij}) \log r_{ij} + g_0 \delta_{ij}$, $J_{ij}^{+-} = J_{ij}^{-+} = g'_{ij}(1 - \delta_{ij}) \log r_{ij} + g_1 \delta_{ij}$. Now we again make the mean-field approximation for the long-ranged logarithmic interaction. Again similar to the clean case, for $i \neq j$ we approximate $g \log r_{ij} \sim g' \log r_{ij} \sim \log \Lambda$, knowing that $g, g' \sim 1$ and assuming that average inter-vortex distance is of the same order of magnitude as the system size Λa , and for the core energy we likewise get $g_0, g_1 \sim \log a/\epsilon \sim -\log \epsilon \sim \log \Lambda$. The result is that all terms in $J_{ij}^{\alpha\beta}$, both for $i \neq j$ and $i = j$, are on average of the order $\log \Lambda \gg 1$, and the mean-field approach is justified. We will sometimes denote the 2×2 matrices in the flavor space by hats (e.g. $\hat{J} = J^{\alpha\beta}$).

The Hamiltonian (18) has been obtained starting from the XY model with random couplings J_{ij} , a well-known toy model for studying disordered systems. However, there are several twists. First of all, we do not in fact consider the full XY model: we immediately rewrite it in terms of Coulomb-like vortex interaction, and on top of that we approximate the logarithmic potential energy with a constant all-to-all vortex coupling. This is justified in our case as we mainly study the light patterns which have prominent vortices but it remains an approximation. The all-to-all (infinite range) approximation is ubiquitous in disordered systems and lies at the heart of the solvable Sherington-Kirkpatrick Ising random coupling model [36]. It is certainly not equivalent to considering the XY model with full phase dynamics. Second, we have a two-flavor model which makes it more difficult and is an open problem as far as we know (this is also the reason why we simplify the Hamiltonian drastically in comparison to the microscopic equations). Finally, the random couplings J_{ij} are not centered at zero in our case but at some finite value \bar{J}_{ij} , so we have an additional term linear in the charges $Q_{i\alpha}$. This is obviously equivalent to having an additional random field term, so we have both random couplings and random field.

It is known that the single-flavor Sherington-Kirkpatrick model (with random couplings, at zero field) exhibits a transition between the high-temperature disordered phase, and the low-temperature phase which exhibits the glassy

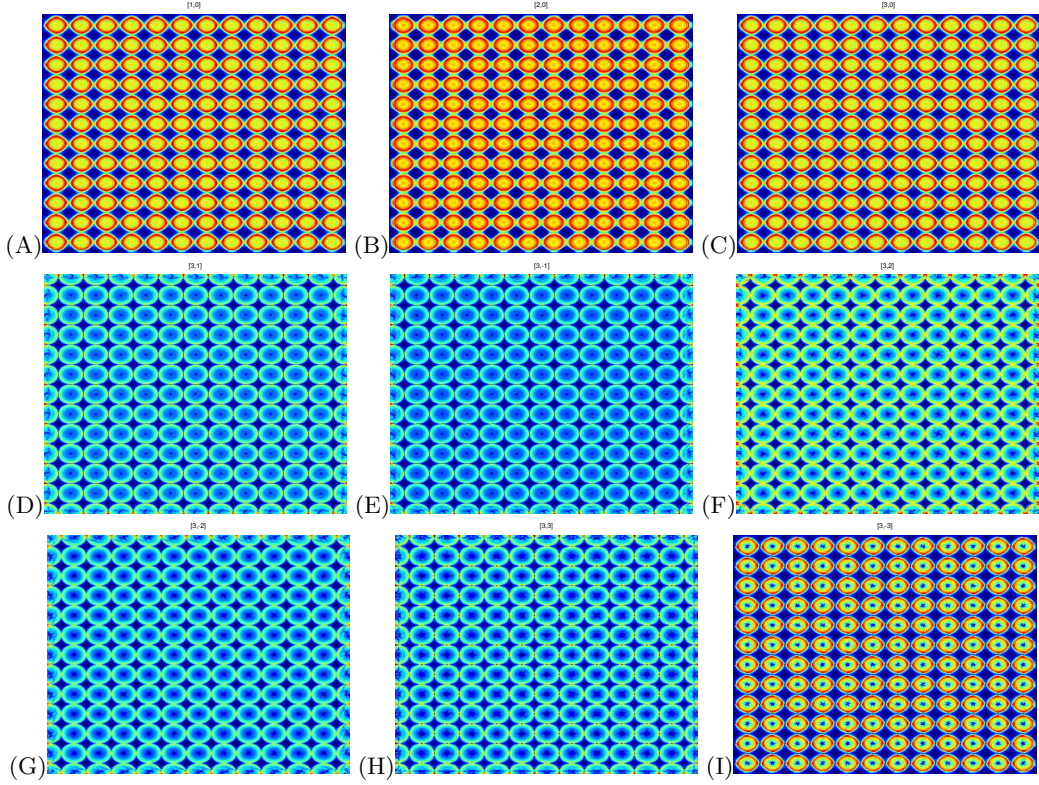


FIG. 8: Vortex lattices with different charges in the FI phase. In the first row (A-C) we see how the CI gets stronger and stronger as the total vortex core energy grow (with the square of the total charge). The second and third row show the growth of CI from $(3, 0)$ to $(3, \pm 3)$ (notice the increasingly reduced intensity in the center and the strong ring-like structure of the beams) but also the forward-backward interaction which favors the configurations $(3, -3)$, $(3, -2)$, $(3, -1)$ over $(3, 3)$, $(3, 2)$, $(3, 1)$. In particular, the $(3, -3)$ lattice is the optimal configuration of all $(3, Q_-)$ configurations even though it has greater CI than say $(3, 0)$ (notice the small dark regions in the center), because the $\sum_{ij} gg' Q_{i+} Q_{i-} \log r_{ij}$ term minimizes the EI – notice there is no "spilling" of intensity from one vortex to the next. The parameters are $\Gamma I = 20$, $L = 2.5\text{mm}$. The lattice parameters are as in the Fig. 6.

long-range correlations. However, what happens in the presence of two flavors and random field in addition to random couplings is far from clear. Random-field XY model with infinite-range couplings is relatively well understood by now [39, 41] but again not in the multi-flavor version nor in combination with random couplings. Below we will try to obtain at least a crude understanding but we do not aspire to solve the model in any rigorous way.

The Gaussian distribution of defects reads $p(J_{ij}^{\alpha\beta}) = \exp\left(-\left(J_{ij}^{\alpha\beta} - J_0^{\alpha\beta}\right) \left(\hat{\sigma}^{-2}\right)_{\alpha\beta} \left(J_{ij}^{\alpha\beta} - J_0^{\alpha\beta}\right)\right)$, where the second moments are contained in the matrix $\sigma_{\alpha\beta}$, with $\sigma_{+-} = \sigma_{-+}$. In this case we get the replicated partition function

$$\bar{\mathcal{Z}}^n = \int \mathcal{D}[Q_{i\alpha}^{(\mu)}] \int \mathcal{D}[J_{ij}^{\alpha\beta}] \exp \left[-\frac{1}{2} \sum_{i,j=1}^N \sum_{\alpha,\beta} \left(J_{ij}^{\alpha\beta} - J_0^{\alpha\beta} \right) \sigma_{\alpha\beta}^{-2} \left(J_{ij}^{\alpha\beta} - J_0^{\alpha\beta} \right) - \sum_{\mu=1}^n \sum_{i,j=1}^N \sum_{\alpha,\beta} \beta J_{ij}^{\alpha\beta} Q_{i\alpha}^{(\mu)} Q_{j\beta}^{(\mu)} \right]. \quad (19)$$

We can now integrate out the couplings $J_{ij}^{\alpha\beta}$ in (19) and get

$$\bar{\mathcal{Z}}^n = \text{const.} \times \int \mathcal{D}[Q_{i\alpha}^{(\mu)}] \exp \left[\frac{1}{2} \beta^2 \sum_{\mu,\nu=1}^n \sum_{i,j=1}^N \sum_{\alpha,\beta} Q_{i\alpha}^{(\mu)} Q_{i\beta}^{(\nu)} \left(\hat{\sigma}^2 \right)_{\alpha\beta} Q_{j\alpha}^{(\mu)} Q_{j\beta}^{(\nu)} - \beta \sum_{\mu=1}^n \sum_{i,j=1}^N \sum_{\alpha,\beta} J_0^{\alpha\beta} Q_{i\alpha}^{(\mu)} Q_{j\beta}^{(\mu)} \right]. \quad (20)$$

Integrating out the disorder has generated the non-local quartic term proportional to the elements of $\sigma_{\alpha\beta}^2$. This has also introduced the inverse "temperature" β as an additional independent parameter. The partition function can be rewritten in the following way, usual in the spin-glass literature [35, 37]. We can introduce the non-local order

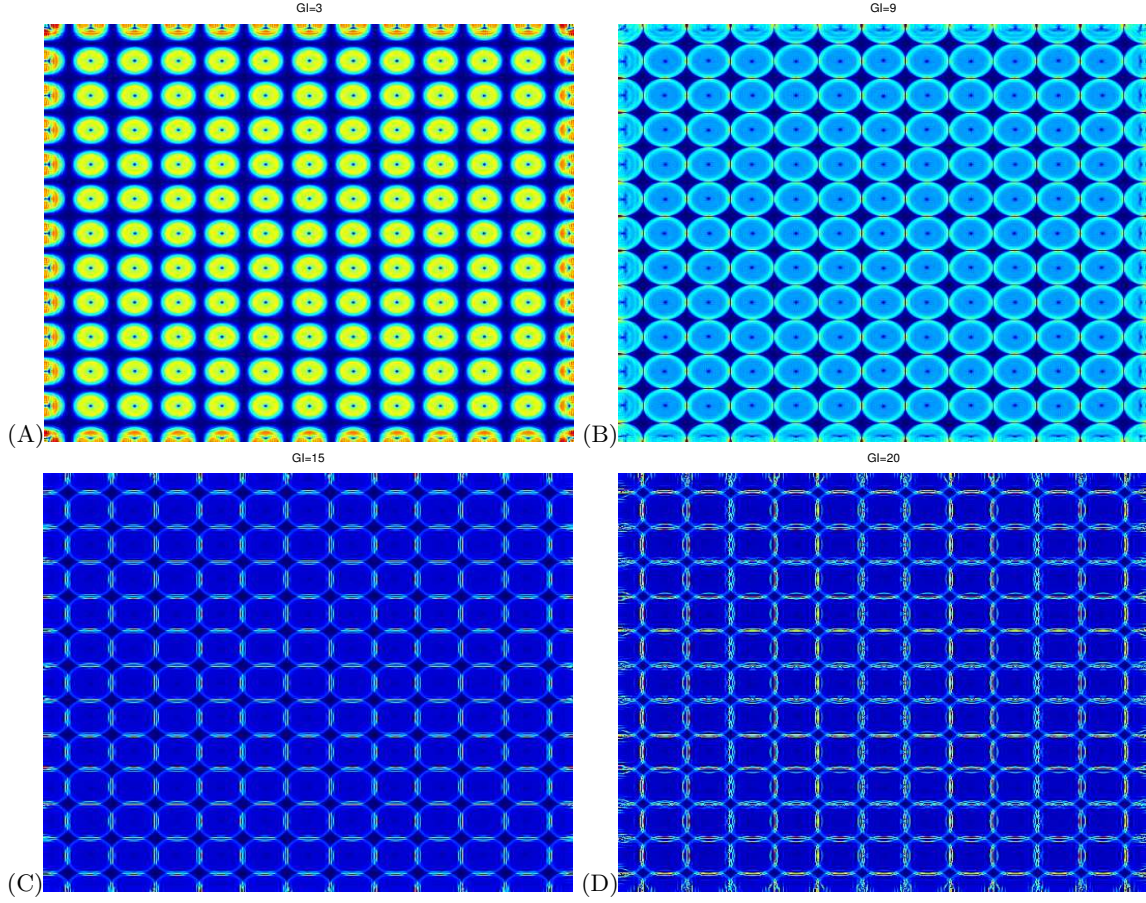


FIG. 9: Intensity maps for the quadratic vortex lattice with charges $(1,1)$, for increasing values of $\Gamma I = \Gamma(I_0 + I_x)$ and $L = 5\text{mm}$. The transition from the PC phase (A, B) into the FI phase (C, D) happens at about $\Gamma I \approx 12$. The edge instability sets in progressively, in accordance with what we saw in the previous figure, leading eventually to an inverse square lattice which looks translationally invariant.

parameter fields

$$p_{\alpha}^{(\mu)} = \frac{1}{N} \sum_{i=1}^N Q_{i\alpha}^{(\mu)}, \quad q_{\alpha\beta}^{(\mu\nu)} = \frac{1}{N} \sum_{i,j=1}^N Q_{i\alpha}^{(\mu)} Q_{j\beta}^{(\nu)}, \quad (21)$$

and the constraints in the replicated partition function $\bar{\mathcal{Z}}^n$:

$$1 \mapsto \int \mathcal{D} [\lambda_{(\mu)}^{\alpha}] \exp \left[\lambda_{(\mu)}^{\alpha} \left(p_{\alpha}^{(\mu)} - \frac{1}{N} \sum_{i=1}^N Q_{i\alpha}^{(\mu)} \right) \right] \quad (22)$$

$$1 \mapsto \int \mathcal{D} [\lambda_{(\mu\nu)}^{\alpha\beta}] \exp \left[\lambda_{(\mu\nu)}^{\alpha\beta} \left(q_{\alpha\beta}^{(\mu\nu)} - \frac{1}{N} \sum_{i,j=1}^N Q_{i\alpha}^{(\mu)} Q_{j\beta}^{(\nu)} \right) \right]. \quad (23)$$

We have five constraints, $\lambda_{(\mu\nu)}^{++}, \lambda_{(\mu\nu)}^{--}, \lambda_{(\mu\nu)}^{+-} = \lambda_{(\mu\nu)}^{-+}, \lambda_{(\mu)}^{+}, \lambda_{(\mu)}^{-}$, for the corresponding five order parameters in (21). We can denote

$$\hat{K} \equiv \begin{pmatrix} \lambda_{(\mu\nu)}^{++} & \lambda_{(\mu\nu)}^{+-} \\ \lambda_{(\mu\nu)}^{+-} & \lambda_{(\mu\nu)}^{--} \end{pmatrix}, \quad \vec{\lambda} \equiv \begin{pmatrix} \lambda_{(\mu)}^{+} \\ \lambda_{(\mu)}^{-} \end{pmatrix}. \quad (24)$$

We will also sometimes leave out the replica indices μ, ν to avoid cramming the notation too much. Now we can first

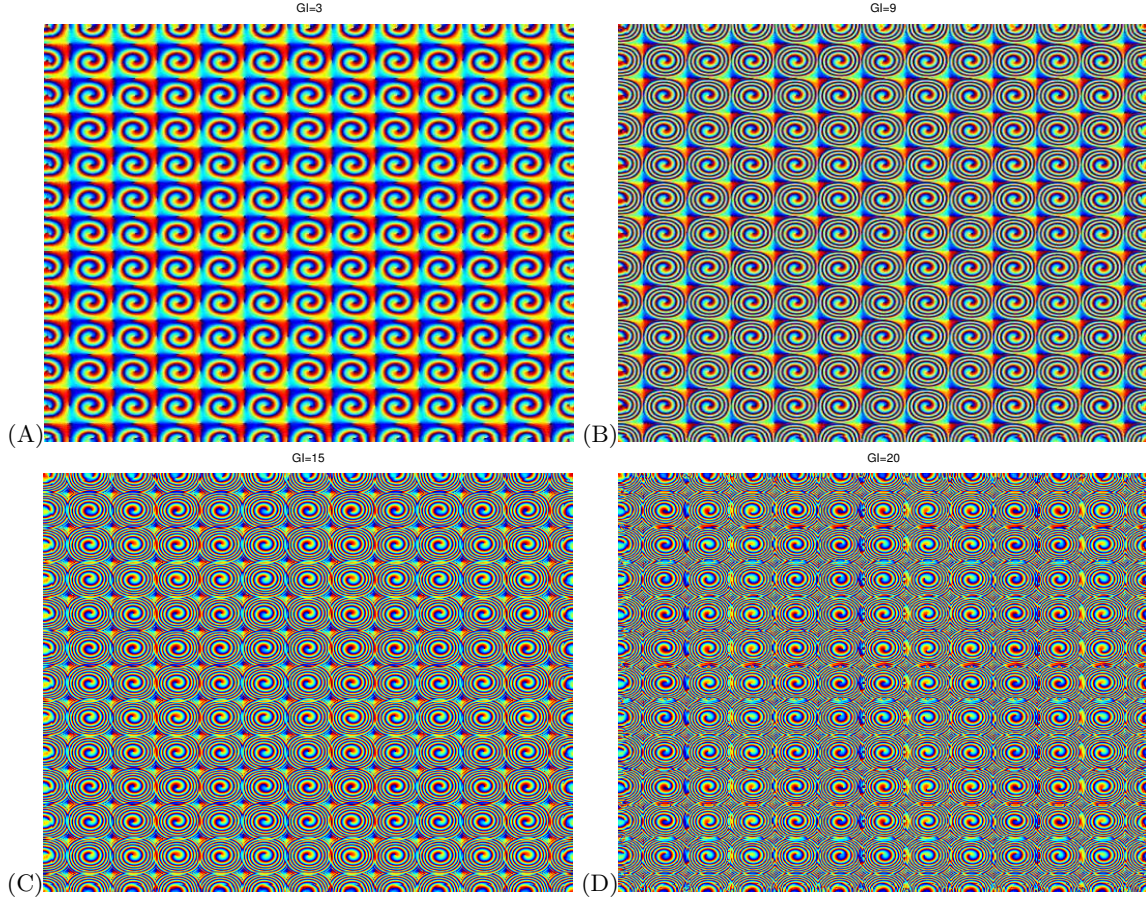


FIG. 10: Phase maps for the F -beam for the same cases as in Fig. 9. As the coupling ΓI grows toward very large values (D), the violation of translation symmetry becomes obvious: notice the vertical and horizontal phase stripes. This instability gives rise to the charge density wave ordering in the presence of disorder.

integrate out the vortex degrees of freedom $Q_{i\alpha}^{(\mu)}$ from (20) to get the effective action

$$\begin{aligned}
 S_{\text{eff}} = & -\frac{\beta^2}{4} \sum_{\mu, \nu=1}^n \left[\sigma_{++}^2 \left(q_{++}^{(\mu\nu)} \right)^2 + 2\sigma_{+-}^2 \left(q_{+-}^{(\mu\nu)} \right)^2 + \sigma_{--}^2 \left(q_{--}^{(\mu\nu)} \right)^2 \right] - \\
 & -\beta \sum_{\mu=1}^n \left[J_0^+ \left(p_+^{(\mu)} \right)^2 + 2J_0^{+-} p_+^{(\mu)} p_-^{(\mu)} + J_0^- \left(p_-^{(\mu)} \right)^2 \right] + \\
 & + \frac{1}{2} \log \det \hat{K} - \frac{1}{4} \vec{\lambda} \hat{K}^{-1} \vec{\lambda} - \\
 & - \sum_{\mu, \nu=1}^n \left(\lambda_{(\mu\nu)}^{++} q_{++}^{(\mu\nu)} + \lambda_{(\mu\nu)}^{+-} q_{+-}^{(\mu\nu)} + \lambda_{(\mu\nu)}^{--} q_{--}^{(\mu\nu)} \right) - \sum_{\mu=1}^n \vec{\lambda}_{(\mu)} \cdot \vec{p}^{(\mu)}. \tag{25}
 \end{aligned}$$

The saddle-point equations for the constraints give the constraints in terms of the expectation values $q^{(\mu\nu)}, p^{(\mu)}$. Luckily, the equation for $\vec{\lambda}$ is easy:

$$\frac{\partial S_{\text{eff}}}{\partial \vec{\lambda}} = \hat{K}^{-1} \vec{\lambda} - \vec{p} = 0, \tag{26}$$

so we immediately solve $\vec{\lambda} = \hat{K}\vec{p}$. Now plugging this into the equations for the three remaining constraints yields

$$\frac{\partial S_{\text{eff}}}{\partial \lambda_{\pm\pm}} = \frac{1}{2} \frac{X \lambda_{\pm\pm}^{-1}}{X^2 - Y^2} - q_{\pm\pm} + \frac{1}{4} (p_{\pm})^2 = 0 \quad (27)$$

$$\frac{\partial S_{\text{eff}}}{\partial \lambda_{+-}} = \frac{Y \lambda_{+-}^{-1}}{X^2 - Y^2} - q_{+-} + \frac{1}{2} p_+ p_- = 0. \quad (28)$$

We have denoted $X = \det \lambda_{++} = \det \lambda_{--}$, $Y = \det \lambda_{+-}$ (these have a well-defined limit in the limit $n \rightarrow 0$). It is trivial to write $\lambda_{\pm\pm}, \lambda_{+-}$ from the above expressions, and we can feed the solutions for all the constraints into the effective action and then solve the saddle-point equations for the order parameters $p_{\pm}, q_{++}, q_{--}, q_{+-}$. Full equations are too complex to be solved, even approximately. We will simplify the problem with the following reasoning. The sums over single-replica order parameters generically scale as $\sum_{\mu} p_{\pm}^{(\mu)} \sim \sum_{\mu} (p_{\pm}^{(\mu)})^2 \sim n$, whereas the double-replica parameters have $\sum_{\mu, \nu} q_{\alpha\beta}^{(\mu\nu)} \sim n^2$. This means that in the limit $n \rightarrow 0$ the p_{\pm} -terms dominate over $q_{\alpha\beta}$ -terms. Therefore, if $p_{\pm} \neq 0$ we can disregard the quantities $q_{\alpha\beta}$ or expand in a series over them, simplifying the equations significantly. Only if the replica symmetry breaking imposes $p_{\pm} = 0$ (not every replica-symmetry-breaking configuration does so), the $q_{\alpha\beta}$ order parameters are significant, and the saddle-point equations with $p_{\pm} = 0$ are again approachable.

Consider first the case $p_{\pm} = 0$. After some algebra, the effective action is now

$$S_{\text{eff}} = -\frac{\beta^2}{4} \sum_{\mu, \nu=1}^n \left(\sigma_{++}^2 (q_{(\mu\nu)}^{++})^2 + 2\sigma_{+-}^2 (q_{(\mu\nu)}^{+-})^2 + \sigma_{--}^2 (q_{(\mu\nu)}^{--})^2 \right) + \frac{1}{2} \log (X^2 |q^{++}|^{-1} \cdot |q^{--}|^{-1} - 4Y^2 |q^{+-}|^{-2}). \quad (29)$$

Consider first the ansatz when the $q^{\pm\pm}$ fields are nonzero, whereas the mixed-flavor field q^{+-} is zero. In this case, the second term in (29), coming from the determinant \hat{K} , simplifies further and we get the saddle-point equation

$$-\frac{\beta^2}{2} \sigma_{\pm\pm}^2 q^{\pm\pm} - \frac{1}{2} (q^{\pm\pm})^{-1} = 0, \quad (30)$$

which is the same as for the infinite-range spin-glass Ising model [35, 37]. One obvious solution is $q^{\pm\pm} = q^{+-} = 0$, the completely disordered system with no vortex proliferation – the familiar insulator phase. It is easy to check that this is indeed a minimum of the effective action S_{eff} . There is also a replica-symmetric but nontrivial solution

$$q_{(\mu\nu)}^{\pm\pm} = \mathcal{Q}_0^{\pm\pm} + (1 - \mathcal{Q}_0^{\pm\pm}) \delta_{\mu\nu}, \quad (31)$$

which yields the solution $\mathcal{Q}_0^{\pm\pm} = 1 - 1/(\beta\sigma^{\pm\pm})$. However, this solution is unstable and is not observable. A stable non-trivial solution is obtained if the replica symmetry is broken. The ansatz is well-known from the spin-glass literature (e. g., [37]) and has a $\rho \times \rho$ matrix $\hat{Q}^{\pm\pm}$ on the block-diagonal and the constant zero elsewhere, with

$$\hat{Q}^{\pm\pm} = \mathcal{Q}_1^{\pm\pm} + (1 - \mathcal{Q}_1^{\pm\pm}) \delta_{\mu\nu}, \quad \mu, \nu = 1, \dots, \rho. \quad (32)$$

Eq. (30) suggests that $\mathcal{Q}_1^{\pm\pm} > 0$ for sufficiently large β , i.e. small L . However, no analytical solution for the elements $\mathcal{Q}_1^{\pm\pm}$ exists and they have to be solved for numerically, by plugging in the solution into the effective action and minimizing it. This is an easy task (for chosen values of the parameters and disorder statistics) but we will not do it here as we do not aim at quantitative accuracy anyway; we merely want to sketch the phase diagram. Now if the third field q^{+-} is nonzero, it satisfies the same equation as (30) just with $\sigma_{++}^2 \mapsto 2\sigma_{+-}^2$. The three combinations of nonzero order parameters correspond to the three familiar phases – $q^{\pm\pm} \neq 0$ is the conductor, $q^{+-} \neq 0$ is the frustrated insulator and $q^{\pm\pm}, q^{+-} \neq 0$ is the perfect conductor.

The solutions with $\vec{p} \neq 0$ yield new physics. In this case, we have at leading order $\lambda_{\pm\pm} = -2X/(X^2 - Y^2)(p^{\pm})^{-2}$, $\lambda_{+-} = -2Y/(X^2 - Y^2)(p^+ p^-)^{-1}$, so the effective action is

$$S_{\text{eff}} = -\beta \sum_{\mu=1}^n \left(J^+ (p_{(\mu)}^+)^2 + 2J^{+-} p_{(\mu)}^+ p_{(\mu)}^- + J^- (p_{(\mu)}^-)^2 \right) - \log p^+ p^- + O(|q^{\alpha\beta}|^2) + O\left(\frac{|q^{\alpha\beta}|}{|\vec{p}|^2}\right), \quad (33)$$

giving the saddle-point equations

$$J^{\pm} p_{(\mu)}^{\pm} + \frac{J^{+-}}{\beta} p_{(\mu)}^{\mp} + (p_{(\mu)}^{\pm})^{-1} = 0, \quad (34)$$

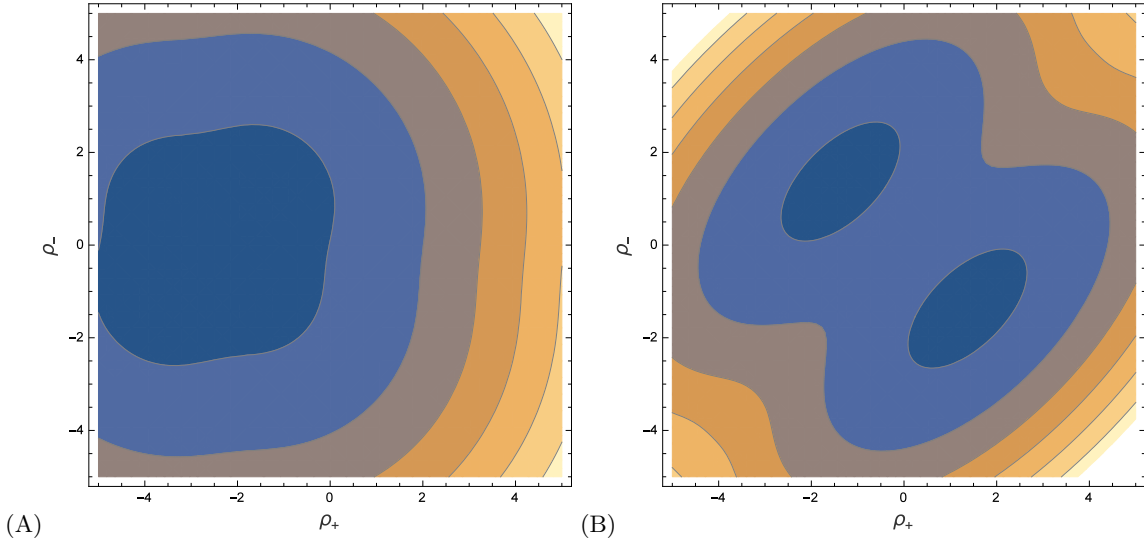


FIG. 11: Free energy (effective action $S_{\text{eff}}^{(\mu)}$) in a given replica subsystem in a photonic lattice with quenched disorder, for the case when the order parameter $p^\pm = \sum_i Q_{i\pm}$ has a nonzero saddle-point solution for the action in a given subsystem (replica). Darker (blue) tones are lower values. The ground states of the system are the local minima. In the panel (A) for $J^+ = -J^- = 1$, there is a single local minimum. In the case (B), for $J^+ = -J^- = 1$, we see two distinct minima of equal height, for two different nonzero values of p^\pm . Such potential energy landscape fits the description of glassy systems.

which easily gives

$$p^\pm = s_1 \sqrt{\frac{1}{J^\pm + s_2 \frac{J^{+-}}{\beta} \sqrt{\frac{J^+}{J^-}}}}, \quad (35)$$

with $s_{1,2} \in \{\pm 1\}$. The solution is the same for every μ and $p_{(\mu)}^\pm = (p^\pm, p^\pm, \dots, p^\pm)$. Now depending on the sign of the determinant $J^+ J^- - (J^{+-})^2$ the solutions for different $s_{1,2}$ may be minima or saddle points. In either case, we have a phase with nonzero local charge density, which is the meaning of \vec{p} . If there are multiple minima we call this phase vortex glass. The reader may argue that true glass should satisfy more stringent conditions and that our phase is not a true glass. Depending on the viewpoint this may well be accepted and we use the term "glass phase" merely as shorter and more convenient than "phase with power-law correlation decay, no long-range order and frustrated free energy landscape". The phase with a single minimum will be called charge density wave, as it has a unique ground state configuration yielding macroscopically nonzero charge density, i.e. it has a true long-range order. On the other had, with multiple minima the replica-averaged charge density sums to zero. The landscape, i.e. the effective action of the system for given replica (μ) as a function of $p_{(\mu)}^\pm$, is given in Fig. 11 as the density map of the function $S_{\text{eff}}(p^+, p^-)$ dependence for $J^+ = -J^- = 1$ (glassy phase, A) and $J^+ = J^- = 1$ (charge density wave, B). We see that the glassy phase shows two inequivalent minima in each replica, with $s_1 = -s_2 = \pm 1$ in Eq. (35), so the total action, the sum of actions of all replica subsystems, can have one and the same value for many configurations, the definition of a highly frustrated system, one of the reasons we dub this phase glass. The charge density wave only has a single minimum for $s_1 = s_2 = 1$.

We can conclude the analysis of the dirty system stating its six phases:

1. One phase violates both the replica symmetry and the flavor symmetry, breaking it down to identity. We dub this phase *vortex charge density wave* (CDW), as it implies spatial modulation of the vortex charge, leading to nonzero net charge density $\sum_i Q_{i\alpha}^{(\mu)}$ in some parts of the system (the *total* net charge density must still be zero: $\sum_\mu \sum_i Q_{i\alpha}^{(\mu)} = 0$, due to charge conservation). Vortices take their charges from $\mathbb{Z} \otimes \mathbb{Z}$.
2. The second phase violates the replica symmetry in both flavors and reduces the flavor symmetry but does not break it down to identity. Instead, it reduces it to the diagonal subgroup $U(1)_F \otimes U(1)_B \rightarrow U(1)_d$, so it has nonzero density of the vortex charge in a given replica $\sum_i Q_{i+}^{(\mu)} = -\sum_i Q_{i-}^{(\mu)}$. Again, the charge density is locally nonzero but now with an additional constraint resulting in frustration (multiple equivalent free energy minima!). This is thus the dirty equivalent of the frustrated insulator phase and we dub it *vortex glass*, as it has

long-range correlations (because of the logarithmic interactions between charged areas), does not break spatial symmetry and exhibits frustration; its charges are from $\pi_1(U(1)_d) = \mathbb{Z}$.

3. The remaining phases have no nonzero net vortex charge density (even locally), and are similar to the phases in the clean system. Vortex perfect conductor violates the replica symmetry of all three fields q^{++}, q^{--}, q^{+-} and allows free proliferation of vortices with charges $(Q_+, Q_-) \in \mathbb{Z} \otimes \mathbb{Z}$.
4. Frustrated vortex insulator preserves the replica symmetry of $q^{\pm\pm}$ but has non-zero value, with broken replica symmetry, of the mixed q^{+-} field, which gives $U(1)_d$ vortices, with charges $Q_+ = -Q_- \in \mathbb{Z}$.
5. Vortex conductor preserves the replica symmetry of the mixed q^{+-} order parameter but violates it in $q^{\pm\pm}$, resulting in the proliferation of single-flavor vortices with \mathbb{Z} charge.
6. Vortex insulator fully preserves the replica symmetry, all order parameters are zero and vortices cannot proliferate.

The phase diagram (given in Fig. 12 in the next subsection) now contains five (six) phases: CDW, insulator (as the special case of CDW for zero disorder), FI, conductor, PC and the glassy phase. The insulator phase is now of measure zero in the (g, g', σ^2) plane, existing only for the points at $\sigma^2 = 0$; for generic nonzero values we have a CDW. For simplicity, we have plotted the phase diagram for $\sigma_{++}^2 = \sigma_{--}^2 = \sigma_{+-}^2 \equiv \sigma^2$.

B. RG analysis and the phase diagram

To study the RG flow, we can start from the replicated partition function (20), inserting the definition of the couplings $J_{ij}^{\alpha\beta}$ and keeping the vortex charges $Q_{i\alpha}^{(\mu)}$ as the degrees of freedom (without introducing the quantities $p_{\alpha}^{\mu}, q_{\alpha\beta}^{(\mu\nu)}$). The basic idea is the same: we consider the fluctuation $\delta(\bar{Z}^n)$ upon the creation of a vortex pair at $\mathbf{r}_{1,2}$ with charges $\vec{q}_1^{(\mu)}, -\vec{q}_2^{(\mu)}$, in the background of the vortices $\vec{Q}_{1,2}^{(\nu)}$ at positions $\mathbf{R}_{1,2}$. Likewise, we introduce the fugacity parameter $y^{(\mu)}$ to account for the vortex core energy. However, this problem is much harder than the clean problem and one has to resort to many approximations to perform the calculation. In its most general form, the problem is still open, in the sense that all known solutions suppose a certain form of replica symmetry breaking or truncate the RG equations [37]. The RG analysis is thus less useful in the disordered case but at least the numerical integration of the flow equations is supposed to give a more precise rendering of the phase diagram compared to the mean field theory.

The starting Hamiltonian is the same as in (20). Now we will write it out more explicitly, keeping the distance-dependent parts:

$$\beta\mathcal{H}_{\text{eff}} = \beta \sum_{\mu=1}^n \sum_{i,j} \left(\bar{g}_c \vec{Q}_i^{(\mu)} \cdot \vec{Q}_j^{(\mu)} + \bar{g}'_c \vec{Q}_i^{(\mu)} \times \vec{Q}_j^{(\mu)} \right) \log r_{ij} - \frac{\beta^2}{2} \sum_{\mu,\nu=1}^n \sum_{i,j} Q_{i\alpha}^{(\mu)} Q_{i\beta}^{(\nu)} \sigma_{\alpha\beta}^2 Q_{j\alpha}^{(\mu)} Q_{j\beta}^{(\nu)}. \quad (36)$$

We have denoted the elements of J_0 by $J_0^{++} = J_0^{--} = \bar{g}_c$, $J_0^{+-} = J_0^{-+} = \bar{g}'_c$ (the bars over the letter remind us that these are disorder-averaged values). The fluctuation of the partition function is completely analogous to the clean case, only it has the additional non-local quartic term. It can again be expanded over r_{12} as in (14) but the quartic term contains no small parameter for the power series expansion and has to be kept in the exponential form. Starting from the expression for the fluctuation analogous to the clean case (14), we get

$$\begin{aligned} \frac{\delta \mathcal{Z}}{\mathcal{Z}} = 1 + \frac{y^4}{4} \sum_{\vec{q}^{(\rho)}, \vec{q}^{(\sigma)}} e^{-\frac{\beta^2}{2}(\vec{q}^{(\rho)}, -\vec{q}^{(\sigma)}, \vec{q}^{(\rho)}, -\vec{q}^{(\sigma)}) + \frac{\beta^2}{2}(\vec{Q}^{(\mu)}, \vec{q}^{(\rho)}, \vec{Q}^{(\nu)}, \vec{q}^{(\sigma)})} \int d\mathbf{r}_{12} r_{12}^3 e^{g\vec{q}^{(\rho)} \cdot \vec{q}^{(\rho)} + g' \vec{q}^{(\rho)} \times \vec{q}^{(\rho)}} \times \\ \times \left[\int d\mathbf{r} r^2 \left(g \vec{Q}_1^{(\mu)} \cdot \vec{q}^{(\rho)} + g' \vec{Q}_1^{(\mu)} \times \vec{q}^{(\rho)} \right) \nabla \log |\mathbf{R}_1 - \mathbf{r}| + \left(g \vec{Q}_2^{(\mu)} \cdot \vec{q}^{(\rho)} + g' \vec{Q}_2^{(\mu)} \times \vec{q}^{(\rho)} \right) \nabla \log |\mathbf{R}_2 - \mathbf{r}| \right]^2. \end{aligned} \quad (37)$$

We have used the notation:

$$(\vec{q}_1, \vec{q}_2, \vec{q}_3, \vec{q}_4) \equiv \sigma_{++}^2 q_1 + q_3 + q_2 + q_4 + \sigma_{+-}^2 (q_1 + q_3 - q_2 + q_4 + q_1 - q_3 + q_2 - q_4) + \sigma_{--}^2 q_1 - q_3 - q_2 - q_4. \quad (38)$$

Now we trace out the fluctuations first by integrating over r and doing some simple algebra:

$$\begin{aligned} \frac{\delta \mathcal{Z}}{\mathcal{Z}} = & \left[1 + 16y^4 (g + g')^2 \cosh(\beta^2 \sigma_{++}^2 + \beta^2 \sigma_{+-}^2) \cosh(\beta^2 \sigma_{-+}^2 + \beta^2 \sigma_{--}^2) \left(\vec{Q}_1^{(\mu)} \cdot \vec{Q}_2^{(\nu)} + \vec{Q}_1^{(\mu)} \times \vec{Q}_2^{(\nu)} \right) \log R_{12} \right] \times \\ & \times \left[1 + 16y^4 (g - g')^2 \cosh(\beta^2 \sigma_{++}^2 - \beta^2 \sigma_{+-}^2) \cosh(\beta^2 \sigma_{-+}^2 - \beta^2 \sigma_{--}^2) \left(\vec{Q}_1^{(\mu)} \cdot \vec{Q}_2^{(\nu)} - \vec{Q}_1^{(\mu)} \times \vec{Q}_2^{(\nu)} \right) \log R_{12} \right] \times \\ & \times \left[1 - 2\pi y^4 e^{-\frac{\beta^2}{2} \left(\sigma_{++}^2 (q_+^{(\mu)} q_+^{(\nu)})^2 + \sigma_{+-}^2 (q_+^{(\mu)} q_-^{(\nu)})^2 + \sigma_{-+}^2 (q_-^{(\mu)} q_+^{(\nu)})^2 + \sigma_{--}^2 (q_-^{(\mu)} q_-^{(\nu)})^2 \right)} \int dr r^{1-\beta} (g \vec{q}^{(\mu)} \cdot \vec{q}^{(\nu)} + g' \vec{q}^{(\mu)} \times \vec{q}^{(\nu)}) \right] \end{aligned} \quad (39)$$

The next step is the summation over all possible ± 1 charges of virtual vortices $\vec{q}^{(\mu)}, \vec{q}^{(\nu)}$ (the two replica indices mean two summations from 1 to n), which requires quite some algebra. The renormalized partition function $\bar{\mathcal{Z}}^n$ finally gives the RG flow equations:

$$\begin{aligned} \frac{\partial g}{\partial \ell} &= -8\pi (g + g')^2 y^4 \cosh(\beta^2 \sigma_{++}^2 + \beta^2 \sigma_{+-}^2) \cosh(\beta^2 \sigma_{-+}^2 + \beta^2 \sigma_{--}^2) - \\ &\quad - 8\pi (g - g')^2 y^4 \cosh(\beta^2 \sigma_{++}^2 - \beta^2 \sigma_{+-}^2) \cosh(\beta^2 \sigma_{-+}^2 - \beta^2 \sigma_{--}^2) \\ \frac{\partial g'}{\partial \ell} &= -\pi (g + g')^2 y^4 \cosh(\beta^2 \sigma_{++}^2 + \beta^2 \sigma_{+-}^2) \cosh(\beta^2 \sigma_{-+}^2 + \beta^2 \sigma_{--}^2) - \\ &\quad - \pi (g - g')^2 y^4 \cosh(\beta^2 \sigma_{++}^2 - \beta^2 \sigma_{+-}^2) \cosh(\beta^2 \sigma_{-+}^2 - \beta^2 \sigma_{--}^2) \\ \frac{\partial y}{\partial \ell} &= 2\pi \left(1 - g - g' - \frac{\beta^2}{4} (\sigma_{++}^2 + 2\sigma_{+-}^2 + \sigma_{--}^2) \right) y \\ \frac{\partial \sigma_{\alpha\beta}^2}{\partial \ell} &= -2\pi \beta^4 \sigma_{\alpha\beta}^4 y^4. \end{aligned} \quad (40)$$

A fixed point lies either at infinite y or at $y = 0$, depending on the combination $g + g' + \beta^2 \sigma^2$ in the equation for $\partial y / \partial \ell$ (for simplicity, we consider again the case where $\sigma_{\alpha\beta}^2$ are all equal).

1. When the fugacity flows toward infinity, we reproduce the phases and the fixed point values (g, g', σ^2) from the clean case: the PC flows toward $(0, 0, 0)$, the FI toward $(g_*, g'_*, 0)$ and the conductor toward $(g_*, g'_{**}, 0)$ with $g_* \rightarrow -\infty, g'_* \rightarrow -\infty, g'_{**} \rightarrow \infty$. Notice that all these phases flow to $\sigma^2 = 0$, i.e. disorder is irrelevant.
2. When the fixed point lies at $y = 0$, one possibility is that all parameters (g, g', σ^2) flow toward some non-universal nonzero values. The attraction region of this point is the CDW phase: the disorder term stays finite as well as the couplings. In particular, the points on the half-plane $g + g' > 0, \sigma^2 = 0$ stay at $\sigma^2 = 0$ (with constant coupling values) and this is the insulator phase from the clean case. Notice that $\sigma^2 > 0$ now, i.e. disorder is relevant. For $\sigma^2 < 1$, this are the only fixed points when $y = 0$.
3. However, for sufficiently strong disorder ($\sigma^2 > 1$), there is a new line of fixed points at $y = 0$ with a finite attraction region, corresponding to a new phase. For $\beta > 1$, the right-hand side of the second RG equation in (40) has a zero at nonzero g' and there are trajectories flowing toward $(y, g, g', \sigma^2) = (0, g, g'(g), \sigma^2(g))$ and not toward an arbitrary nonuniversal value of σ^2 . This is precisely the glass phase, where disorder is again relevant. At the lowest order, the relation between g, g', σ^2 at the fixed point line is given by the relation $g + g' + \beta^2 \sigma^2 = 1$.

Now we have made contact between the mean-field classification of phases and the fixed points and regions of the RG flow. The flows in the (g, g') plane are given in the Fig. 12. The parameter space is four-dimensional so the phase structure is different at different disorder concentrations σ^2 . In the (A) panel for $\sigma^2 = 0.4$, the phase structure is similar to the clean case – we see the same four phases except that insulator (no stable vortices) is replaced by the CDW phase. In the (B) panel, for $\sigma^2 = 1.2$, the CDW phase is replaced by another disordered phase, the glass-like regime. Importantly, the glass phase does not cross the $g' = 0$ axis, meaning that a single-flavor system even with disorder could not support a glass. We thus conjecture that the transition at $\sigma^2 = 1$ is of first order, as the change is the structure of the (g, g') phase diagram is discontinuous, and we do not see how this could happen if the first derivative $\partial \mathcal{F} / \partial \rho_{\pm}$ (the derivative of the free energy with respect to vortex charge density) is continuous. However, we have not checked the order of this transition by explicit calculation. The phase structure is further seen in the $\sigma^2 - g'$ diagram, where we see the glass phase emerge at some value of the disorder. This is discussed further in the next section, where we study the equivalent antiferromagnetic system (with the same structure of the phase diagram, Fig. 17).

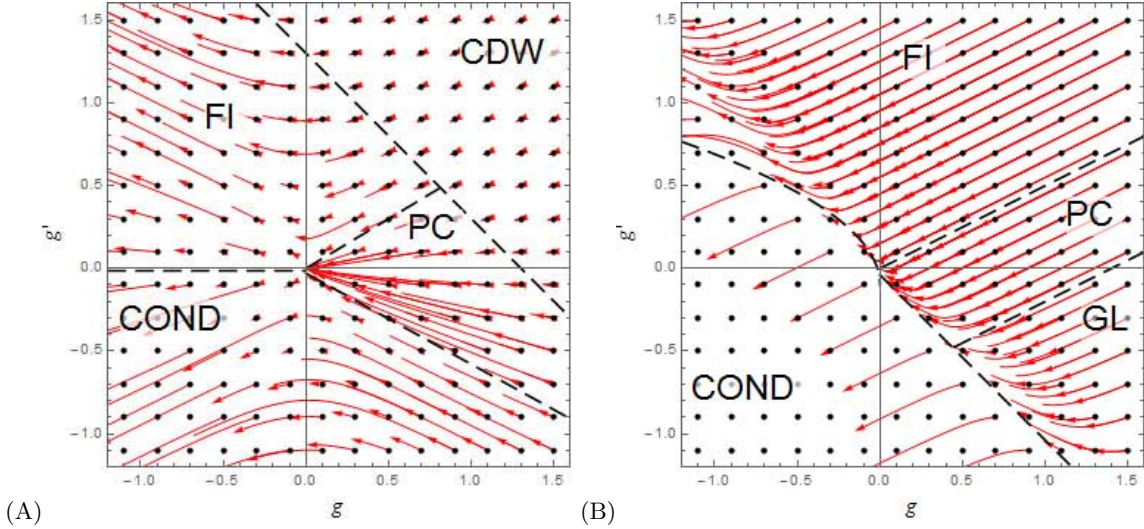


FIG. 12: Phase diagram for the system with lattice disorder in the g - g' plane together with RG flows, with red lines denoting the flows starting at the initial conditions denoted by black points. The dashed black lines are approximate phase boundaries from mean-field theory, and the parameters are $\sigma^2 = 0.4, L = 3.0, \beta = 1/L = 0.33$ and $\sigma^2 = 0.4$ (A) and $\sigma^2 = 1.2$ (B). In (A), the area where $g + g' + \beta^2 \sigma^2 > 1$ is inhabited by the flows toward nonuniversal values of (g, g') which belong to the CDW phase and the opposite region is divided between the attraction regions of $(0, 0)$, $(g_* \rightarrow \infty, g'_* \rightarrow \infty)$ and $(g_{**} \rightarrow \infty, g'_{**} \rightarrow -\infty)$ – the familiar PC, FI and conductor phases. In the panel (B), for $\sigma^2 = 1.2$, the disorder becomes relevant in the glass phase (denoted by "GL"), whose RG flows end on the half-line of fixed points $g + g' + \beta^2 \sigma^2 = 1, g' < 0$. For our parameter values this line happens to pass almost through the origin; in general this is not necessarily the case. The non-disordered phases (flowing to $\sigma^2 = 0$) – FI, conductor and PC have survived.

C. Geometry of patterns

The two previously considered mechanisms of instability – central instability and edge instability – remain active also in the presence of disorder. However, in the presence of disorder there is a third, inherently collective effect that we dub *domain instability* (DI). It follows from the fact that the self-focusing term ΓE grows with intensity I : more illuminated regions react faster (Eqs. 1-2). In the presence of lattice there is a relatively large region of initially zero intensity, whereas the regular lattice cells have some nonzero intensity I . Approximating I with a constant, our equations in the vicinity of the defect (hole) in the lattice becomes the Schrödinger equation in a step potential, so the z -dependent part of the solution is of the form $\sum_k e^{i\lambda_k z}$ and the eigenenergies along z are gapped by the inverse length: $\lambda_k > 1/L$. For small energies, the transmission coefficient is very low whereas for large energies it approaches unity. Thus for $1/L$ large, i.e. β small most of the intensity remains confined by the borders of the defect and the intensity does not spill but for small $1/L$ the beam profile is deformed by the "spilling" into the hole regions. For vortices, there is an additional Coulomb interaction in the $x-y$ plane, meaning the effective potential is not piecewise constant anymore (even in the simplest approximation) but the qualitative conclusion remains: large L brings global reshaping of the intensity profile.

The other phases are analogous to the ones in the clean case, though with a general trend that the presence of disorder decreases the stability of vortex patterns. The PC and FI phases are shown in Figs. 13-14. In this section we only look at the lattices, as the notion of disorder is inapplicable for a single beam. Consider first the patterns in the PC phase (Fig. 13). Compared to the clean case (Fig. 6(A)), the symmetry is much reduced, from $O(2)$ to C_4 but the vortices are conserved and the original lattice structure (outside the wholes) is clearly visible. The FI (Fig. 14) shows mainly EI (and to a smaller extent CI), which together lead to the lattice inversion. The rule of thumb for differentiating the conductor and PC on one side from the CDW and FI on the other side is precisely the presence of the lattice inversion. The absence of the charge transport is best appreciated in the phase images: the charge pins to the defects and localizes toward the end of the crystal (i. e., for z near L). Only near the edges we see high vorticity, somewhat analogous to topological insulators, which only have nonzero conductivity along the edges of the system.

The CDW versus the glass phase is given in Fig. 15. The charge density wave (A, C, $L = 240\mu\text{m}$) exhibits the diffusion of intensity due to DI, and the vortex beams are in general asymmetric and not clearly delineated. In (B, D), where $L = 120\mu\text{m}$ with all other parameters the same, there is a clear border between defects and the regular parts of the lattice and the intensity is concentrated in the vortex cores. We give also the vortex charge density map in (C,D) in addition to the intensity maps in (A,B) as the charge density shows why the CDW is insulating: even though

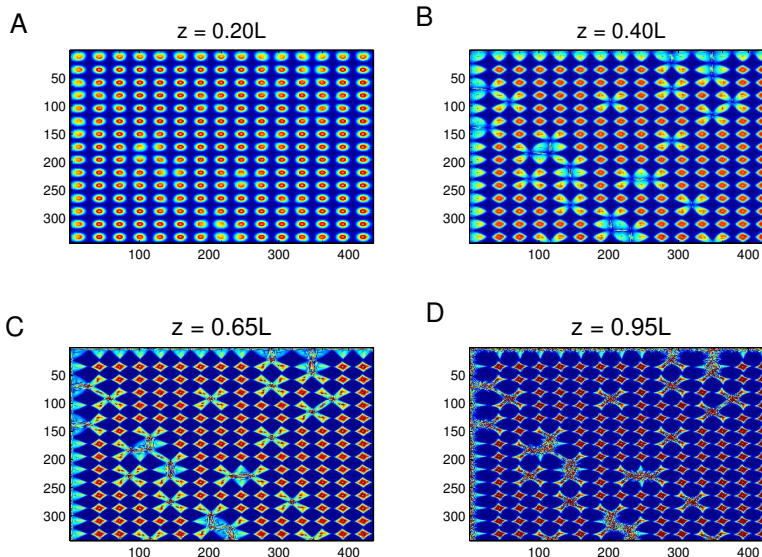


FIG. 13: The PC phase in a Gaussian beam lattice on a background lattice with $\sigma^2 = 0.1$, $\Gamma I = 20$, $L = 2\text{mm}$, FWHM for the CP beams is $9\mu\text{m}$ and for the photonic lattice $6\mu\text{m}$. The vortex charge is $(1,1)$ which is sufficiently low that the CI does not destroy the vortices. We see some CI-induced symmetry reduction from $O(2)$ to C_4 but the overall lattice structure is preserved.

individual beams diffuse and smear out in *intensity*, the regions of nonzero vortex charge are disjoint and no global conduction can occur. Glass is divided into ordered domains in intensity but the vortex charges form a connected network which supports transport. This is analogous to the percolation transition in a disordered Ising model [36] and we may expect that the CDW-glass transition follows the same scaling laws near the critical point. However, we have not checked this explicitly and we leave it for further work.

V. THE CONDENSED MATTER ANALOGY: COLLINEAR DOPED HEISENBERG ANTIFERROMAGNET

The two-beam photorefractive system is actually a good model of a quantum magnetic systems. The most obvious connection is to multi-component XY antiferromagnets (i.e., two-dimensional Heisenberg model): planar spins are nothing but complex scalars, and the Lagrangian remains identical, together with the vortices ($\pi_1(SO(2)) = \pi_1(U(1)) = \mathbb{Z}$). The nonlinearity in the spin system is different and usually much simpler, but that typically does not influence the phase diagram (the symmetry structure remains the same). Such connection is so obvious it does not require further explanations. Our point is that the CP beams in a PR crystal can also describe more general magnetic systems in the presence of topological solutions described by groups different than \mathbb{Z} . In particular, we want to point out to a connection with a two-sublattice antiferromagnetic system which has some time ago enjoyed considerable popularity as a possible description of the magnetic ordering in numerous planar strongly-coupled electron systems, including cuprate high- T_c superconductors [5, 33, 42]. This is the collinear doped antiferromagnet defined on two interpenetrating sublattices. When coupled to a charge density wave (speaking about the usual, $U(1)$ electromagnetic charge) and a superconducting order parameter, it becomes a toy model of cuprate materials (one variant is given in [42]). In the light of what we know today, the ability of this model to describe the cuprate physics realistically is quite questionable; but even so it is an interesting magnetic system on its own, and above all was already found in [43, 44] to exhibit a spin-glass phase, though in a slightly different variant (in particular, with spiral instead of collinear ordering).

Let us formulate the model. While the material is a lattice on the microscopic level, here we are talking about an effective field theory model. The order parameter is the staggered magnetization

$$M(\mathbf{r}) = \sum_{\alpha=1,2} \mathbf{M}_\alpha(\mathbf{r}) \cos(\mathbf{n} \cdot \mathbf{r}), \quad (41)$$

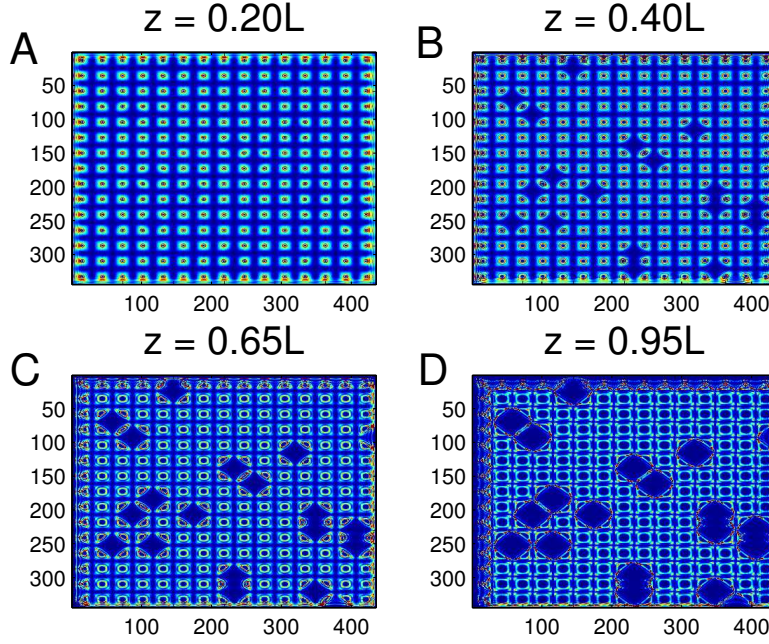


FIG. 14: The FI phase in the same lattice as above but with $\Gamma I = 40$. Now both the CI (low-intensity regions in the beam center in A,B) and the EI (lattice inversion in C,D) are present. The net result is the lattice inversion, and the vortex charge dissipates along the inverse lattice.

where $\alpha \in \{1, 2\}$ is the sublattice "flavor" index (analogous to the $\{F, B\}$ index in the previous sections) and each component \mathbf{M}_α is a three-component spin, describing the internal, i.e. spin degree of freedom (we label the spin axes as X,Y,Z). The total spin is thus the sum of the spins of the two components, and \mathbf{n} is the modulation vector. The modulation gives rows of alternating staggered magnetization in opposite directions as in Fig. 16 (panel (A) and zoom-in in panel (C)). This stands in contrast with the spiral order, where the modulation vectors become \mathbf{n}_α , i.e. differ for the two sublattices, and are themselves space-dependent [43]. The ordered phase of the collinear system has the nonzero expectation value of the staggered magnetization along one direction, which can be chosen as the Z-axis ("easy axis"), where the spin fluctuations about the easy axis remain massless, and the symmetry is broken from $O(3)$ to $O(3)/O(2)$. The spiral order, on the other hand, breaks the symmetry down to identity, as the order parameter is a dreibein [43].

The symmetry conditions (isotropy in absence of external magnetic field) determine the Hamiltonian up to fourth order, as discussed in [42]:

$$\mathcal{H}_{\text{af}} = \frac{1}{2g_M} \left[\left(\frac{1}{c_M} \partial_\tau \mathbf{M}_\alpha \right)^2 + |\nabla \mathbf{M}_\alpha|^2 + \frac{r}{2} |\mathbf{M}_\alpha|^2 \right] + \frac{u_0}{2} |\mathbf{M}_\alpha|^4 - v_0 (|\mathbf{M}_1|^2 + |\mathbf{M}_2|^2)^2. \quad (42)$$

The antiferromagnetic coupling is g_M , the spin stiffness is c_M , the mass r and the fourth-order coupling u comes from the "soft" implementation of the constraint $|\mathbf{M}_\alpha| = 1$ [53] and v is the anisotropy between the two sublattices, justified by the microscopic physics [5, 42]. The Hamiltonian can be transformed by rescaling τ and x, y , together with the couplings u and v to set $g_M = c_M = 1$ so that the kinetic term becomes isotropic, giving

$$\mathcal{H}_{\text{af}} = \frac{1}{2} (\partial_\tau M)^2 + \frac{1}{2} |\nabla M|^2 + \frac{r}{2} |M|^2 + \frac{u}{2} (|M|^2)^2 - v |\mathbf{M}_1|^2 |\mathbf{M}_2|^2, \quad (43)$$

where we have also rewritten the quartic terms for convenience. Without anisotropy, the energy of the system is a function of $|\mathbf{M}_1|^2 + |\mathbf{M}_2|^2$ only and the symmetry group is the full $O(6)$. With $v \neq 0$, the symmetry is reduced to $O(3)_1 \otimes O(3)_2$: the internal spin symmetry in each sublattice remains unbroken but the spatial rotation symmetry between the layers is broken down to just the discrete flip. Compare this to the $U(1) \otimes U(1)$ symmetry in the PR system: there, it is the internal phase symmetry that remains unbroken.

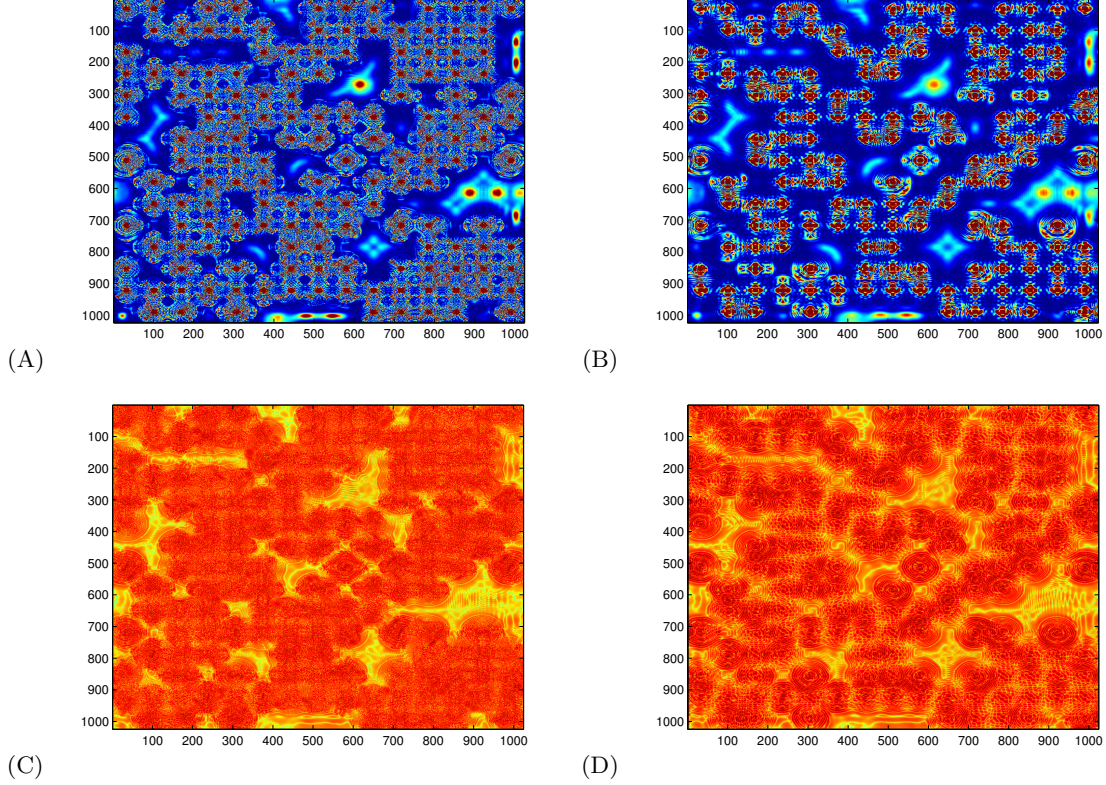


FIG. 15: The charge density wave (A,C) and the glass phase (B,D), intensity maps (left) and vortex charge density map (right). The telltale difference is that the CDW loses the regular lattice as the intensity "flows" between the regular and the defect regions and we see the DI at work. Glass on the other hand consists of domains with well-defined vortices though with reduced symmetry (C_4) mostly due to EI. The charge density forms a connected network in the glass phase and transport is possible, whereas in a frustrated insulator the charge is stuck in isolated points.

A. \mathbb{Z}_2 vortices

Remembering that topological solitons are classified by homotopy groups, and that we work in a two-dimensional plane, the relevant group is again the first homotopy group, $\pi_1(O(3)) = \mathbb{Z}_2$. For simplicity, we will call these excitations vortices, same as for the \mathbb{Z} homotopy group, bearing in mind that the only possible charges are $Q_\alpha = \pm 1$. A realization of the "vortex" with $Q = 1$ is shown in Fig. 16(B). Since the spins are three-dimensional (the figure shows the projection in the XY plane), it becomes clear that higher vortex charges are equivalent to zero charge: winding around twice in the XY plane can be done along a closed line in the XYZ space which can be contracted to a point (in other words, it is continuously deformable to a trivial configuration via a path the crosses the north pole of the π -ball, the group manifold of $SO(3)$). That could not happen for the two-dimensional phase $U(1)$ precisely because there is no extra dimension. In Fig. 16(D) the "vortex" is superimposed onto the regular configuration: it is recognizable as a contact point between two lines of alternating staggered magnetization.

Now let us derive the effective Hamiltonian of the vortices. For the \mathbb{Z}_2 vortex, a loop in real space is mapped onto a π -arc in the internal space, so the vortex can be represented as

$$\mathbf{M}_\alpha(r, \phi) = \int d\phi' e^{\frac{i}{2}(\phi' - \phi)} \hat{\ell}_3 \mathbf{m}_\alpha, \quad (44)$$

giving (the matrices $\ell_{1,2,3}$ represent the $so(3)$ algebra):

$$\mathbf{M}_\alpha = \begin{pmatrix} \cos \phi & \mp \sin \phi & 0 \\ \pm \sin \phi & \cos \phi & 0 \\ 0 & 0 & 1 \end{pmatrix} \begin{pmatrix} m_{1\alpha} \\ m_{2\alpha} \\ m_{3\alpha} \end{pmatrix}, \quad (45)$$

where \mathbf{m}_α is the magnetization amplitude, analogous to the beam amplitude ψ_α in the optical system. The leading-

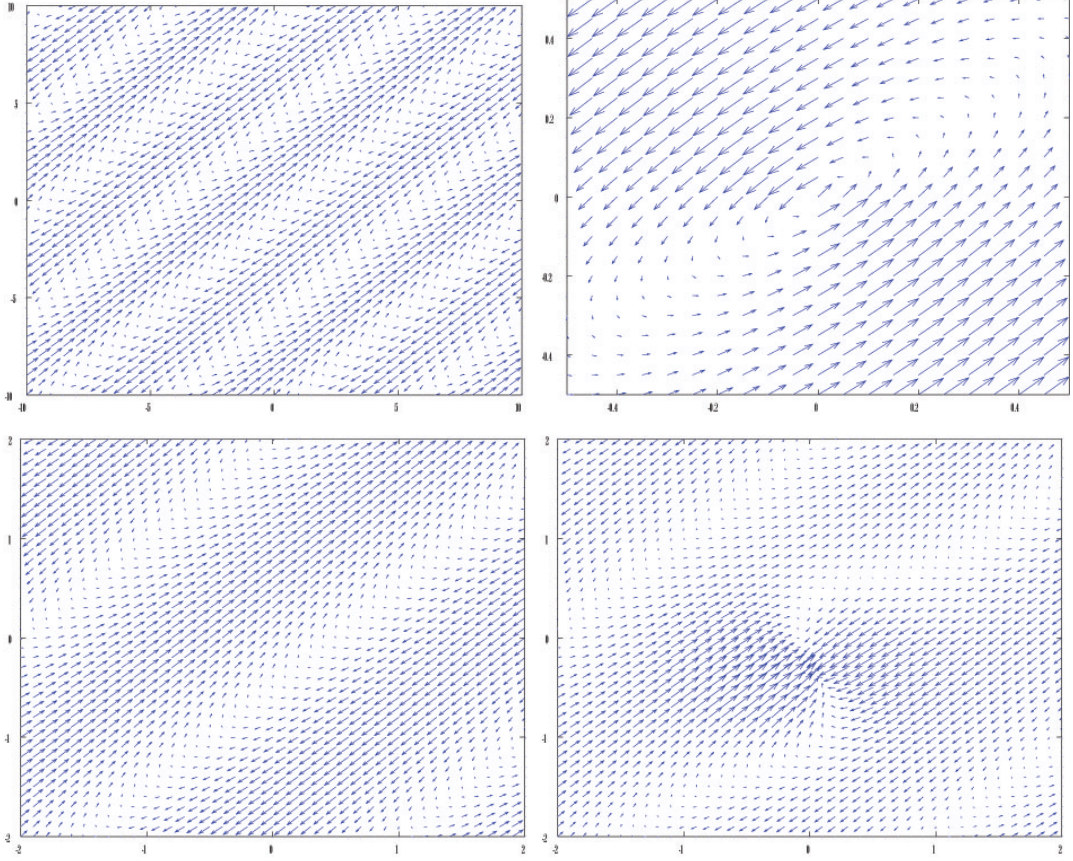


FIG. 16: Numerical realization of a \mathbb{Z}_2 -charged point defect with $Q = 1$ of the staggered magnetization \mathbf{M}_1 . The magnetization is three-dimensional and we show the projection in the XY-plane, $\mathbf{M} \cdot \mathbf{n}_{XY} = M_\perp$. In (A) we see the defect-free configuration, with the characteristic collinear spin pattern from Eq. (41). In (B) we show only the vortex configuration with positive charge, Eq. (45). In (C-D) we plot show how the vortex superimposes onto the background spin texture, zoomed-in compared to the large-scale wave in (A). The parameters are $u = r = 1$ and $v = 0.5$.

order, non-interacting term in (43) gives for the energy of a single vortex of charge \vec{Q} :

$$E_1 = 2\pi(|\mathbf{m}_X \times \mathbf{e}_Z|^2 + |\mathbf{m}_Y \times \mathbf{e}_Z|^2) \log \Lambda = 2\pi|\mathbf{m}_{\perp\alpha}|^2 \log \Lambda, \quad (46)$$

which is in fact independent of \vec{Q} (as could be expected, as it is in general proportional to $\vec{Q} \cdot \vec{Q}$ which is a constant for parity vortices). The vortex singles out an easy axis (Z-axis) around which the staggered magnetization winds (ϕ being the winding angle). This allows one to introduce $\mathbf{m}_{\alpha\perp} \equiv (m_{X\alpha}, m_{Y\alpha}, 0)$. A vortex pair with charges \vec{Q}_i and \vec{Q}_j has the binding energy

$$E_2 = 2\pi\vec{Q}_i \cdot \vec{Q}_j (|\mathbf{m}_1 \times \mathbf{e}_Z|^2 + |\mathbf{m}_2 \times \mathbf{e}_Z|^2) \log r_{ij} = 2\pi|\mathbf{m}_{\perp\alpha}|^2 \vec{Q}_i \cdot \vec{Q}_j \log r_{ij}, \quad (47)$$

which gives a vortex Hamiltonian analogous to (8):

$$\mathcal{H}_{\text{vort}} = \sum_{i < j} \left(g\vec{Q}_i \cdot \vec{Q}_j + g'\vec{Q}_i \times \vec{Q}_j \right) \log r_{ij} + \sum_i \vec{\mu} \cdot \vec{Q}_i. \quad (48)$$

Two obvious differences with respect to the optical system are (i) the charges are now limited to the values ± 1 (ii) there is a term linear in charge density, which acts as a chemical potential. The latter arises from the coupling of the spin waves (i.e., the topologically trivial excitations of the amplitude \mathbf{m}_α) to the vortices. More precisely, it can be traced to the existence of the third, Z-axis of the spin, as opposed to the two-dimensional XY model, and the fact that the spin waves along the Z-spin axis couple to the vortices, i.e. to the winding phase (in the XY spin plane). Proceeding similarly to that derivation (separating the fluctuations of the amplitude and the phase), we find the

microscopic expressions for the effective parameters g, g', μ_α :

$$g = m_\perp^2 + \frac{4r + 6um_\perp^2}{(2v + \frac{3}{2}um_\perp^2 + \frac{v}{2}m_\perp^2)(2r + \frac{3}{2}um_\perp^2 - \frac{v}{2}m_\perp^2)} \quad (49)$$

$$g' = -\frac{4vm_\perp^2}{(2v + \frac{3}{2}um_\perp^2 + \frac{v}{2}m_\perp^2)(2r + \frac{3}{2}um_\perp^2 - \frac{v}{2}m_\perp^2)} \quad (50)$$

$$\mu_\alpha = \frac{1}{2}m_\perp m_z, \quad (51)$$

assuming $m_{1\perp} = m_{2\perp} \equiv m_\perp$. Now the RG calculation is similar to the optical case but the nonzero chemical potential introduces two differences. First, there is obviously the additional term proportional to the total charge of the virtual pair of vortices, $\mu_\alpha(q_{1\alpha} + q_{2\alpha})$. Second, there is no charge conservation as the expectation value of the total vortex charge is now $\langle \vec{Q} \rangle = \partial \mathcal{F} / \partial \vec{\mu} \neq 0$. Thus we need to take into account not only the fluctuations with zero net charge (virtual vortex pairs with charges $\vec{q}_1 \equiv \vec{q}$ and $\vec{q}_2 \equiv -\vec{q}$) but also the situations with arbitrary pairs \vec{q}_1, \vec{q}_2 . This modifies the variation of the partition function from (14-15) to:

$$\begin{aligned} \frac{\delta \mathcal{Z}}{\mathcal{Z}} &= 1 + \frac{y^4}{4} \sum_{\vec{q}_{1,2}} \int dr_{12} r_{12}^3 e^{-g\vec{q}_1 \cdot \vec{q}_2 - g'\vec{q}_1 \times \vec{q}_2 - \vec{\mu} \cdot \vec{q}'} \times \\ &\times \left[\int dr r^2 \left(g\vec{Q}_1 \cdot \vec{q} + g'\vec{Q}_1 \times \vec{q} \right) \nabla \log |\mathbf{R}_1 - \mathbf{r}| + \left(g\vec{Q}_2 \cdot \vec{q} + g'\vec{Q}_2 \times \vec{q} \right) \nabla \log |\mathbf{R}_2 - \mathbf{r}| \right]^2 + \\ &+ \frac{y^4}{4} \sum_{\vec{q}_{1,2}} \int dr_{12} r_{12}^3 e^{-g\vec{q}_1 \cdot \vec{q}_2 - g'\vec{q}_1 \times \vec{q}_2 - \vec{\mu} \cdot \vec{q}_1} \left[\int dr r^2 \left(g\vec{Q}_1 \cdot \vec{q}_0 + g'\vec{Q}_1 \times \vec{q}_0 \right) \log |\mathbf{R}_1 - \mathbf{r}| + \left(g\vec{Q}_2 \cdot \vec{q}_0 + g'\vec{Q}_2 \times \vec{q}_0 \right) \log |\mathbf{R}_2 - \mathbf{r}| \right]^2, \end{aligned}$$

where we have introduced $2\vec{q} \equiv \vec{q}_1 - \vec{q}_2, \vec{q}_0 \equiv \vec{q}_1 + \vec{q}_2$. The mixed term which includes both \vec{q} and \vec{q}_0 vanishes due to isotropy. Matching the terms in the resulting expression with the original Hamiltonian, we find the recursion relations:

$$\begin{aligned} \frac{\partial g}{\partial \ell} &= -16\pi y^4 (g^2 + g'^2) \\ \frac{\partial g'}{\partial \ell} &= -16\pi y^4 g g' \\ \frac{\partial \vec{\mu}}{\partial \ell} &= 0 \\ \frac{\partial y}{\partial \ell} &= (1 - g - g' - \mu_+ - \mu_-) y. \end{aligned} \quad (52)$$

Crucially, the chemical potential does not run which could be guessed from dimensional analysis (it couples to dimensionless charge). This is the same system as (16) up to the trivial rescaling of the coupling constants and the shift of the critical line $g + g' = 1$ in the PR system to the line $g + g' + \mu_+ + \mu_- = 1$. It becomes obvious that the phase diagrams are mapped onto each other.

B. Influence of disorder

The disorder in a doped antiferromagnet comes from electrically neutral metallic grains quenched in the bipartite lattice. Being metallic and neutral, they are naturally modeled as magnetic dipoles \mathbf{X} quenched in the bipartite lattice. This picture stems from the microscopic considerations in [46]. We again assume the Gaussian distribution of the disorder as $p(X) \propto \exp(-|\mathbf{X}|^2/2\sigma_X^2)$. The disorder dipoles are one and the same for both sublattices, so \mathbf{X} has no flavor (sublattice) index. The minimal coupling of the dipoles to the lattice spins $\partial_i \mapsto \partial_i - i\ell_i X_i$ gives

$$\mathcal{H}_{\text{af}} \mapsto \mathcal{H}_{\text{dis}} = \mathcal{H}_{\text{af}} + \nabla \mathbf{M}_\alpha \cdot (\mathbf{X} \times \mathbf{M}_\alpha) + M^2 X^2. \quad (53)$$

Now the replica calculation requires the multiplication of the M field into n copies and performing the Gaussian integral over the disorder. The initial distribution of the disorder $p(X)$ gives rise to two independent Gaussian distributions for the couplings $J_{ij}^{\alpha\beta}$ with dispersion matrix $\sigma_{\alpha\beta}^2$ and for the chemical potential μ_i^α with the dispersion

matrix ξ_α^2 . For simplicity, consider again the case when $\sigma_{\alpha\beta}^2 \equiv \sigma^2$ and $\xi_\alpha^2 \equiv \xi^2$. The resulting Hamiltonian is

$$\begin{aligned} \mathcal{H}_{\text{dis}} = & \sum_{\mu=0}^n \left(\frac{1}{2} |\partial_\tau \mathbf{M}_\alpha^{(\mu)}|^2 + \frac{1}{2} |\nabla \mathbf{M}_\alpha^{(\mu)}|^2 + \frac{u}{2} |\mathbf{M}_\alpha^{(\mu)}|^2 - v |\mathbf{M}_1^{(\mu)}|^2 |\mathbf{M}_2^{(\mu)}|^2 \right) + \\ & + \frac{\sigma^2}{4} \sum_{\mu,\nu=0}^n \left(\nabla \mathbf{M}_\alpha^{(\mu)} \times \mathbf{M}_\alpha^{(\mu)} \right) \cdot \left(\nabla \mathbf{M}_\alpha^{(\nu)} \times \mathbf{M}_\alpha^{(\nu)} \right), \end{aligned} \quad (54)$$

where we have disregarded the logarithmic term ($\sim \log |\mathbf{M}_\alpha^{(\mu)}|$) as it is subleading (and does not influence the phase winding). Now making use of the representation (44) and plugging it in into (54) gives the disorder vortex Hamiltonian

$$\beta \mathcal{H}_{\text{vort}} = \sum_{\mu,\nu=1}^n \sum_{i,j=1}^N \left[\frac{\beta^2}{2} Q_{i\alpha}^{(\mu)} Q_{i\beta}^{(\nu)} Q_{j\alpha}^{(\mu)} Q_{j\beta}^{(\nu)} - \beta Q_{i\alpha}^{(\mu)} J_0^{\alpha\beta} Q_{j\beta}^{(\mu)} + \beta^2 Q_{i\alpha}^{(\mu)} \xi^2 Q_{i\alpha}^{(\nu)} \right] - \sum_{\mu=1}^n \sum_{i=1}^N \beta \xi^2 \mu_0^\alpha Q_{i\alpha}^{(\mu)}. \quad (55)$$

Of course, we could have arrived at the same effective action starting from the vortex Hamiltonian (48), taking the infinite range approximation and identifying $J_{ij}^{\alpha\alpha} = g_{ij} \log r_{ij}$ and similarly for other components of $J_{ij}^{\alpha\beta}$ as we demonstrated for the PR system. The final result has to be same at leading order. Compared to the Hamiltonian for the photonic lattice with disorder in Eq. (25), there are two extra terms, proportional to the dispersion ξ^2 and the mean $\bar{\mu}_0$ of the chemical potential. The former term just introduces the shift $J_0^{\alpha\beta} \mapsto J_0^{\alpha\beta} - \sigma^2/2\beta$ and the latter term, linear in the vortex charges and proportional to the chemical potential, introduces solutions with nonzero net vortex charge density. Looking back at the saddle-point calculation in (21-35), this tells us that the relation between the phase diagrams is the following. The phases with no net vortex charge density – insulator, conductor, frustrated insulator and perfect conductor – remain the same as in the PR system, since both the average coupling value $J_0^{\alpha\beta}$ which gets shifted and the term proportional to the chemical potential μ_α couple only to $\vec{p}^{(\mu)}$. The structure of phases with nonzero $\vec{p}^{(\mu)}$ depends on the zeros of the saddle point equation

$$J^\pm p^\pm + \left(\frac{J^{+-}}{\beta} - \frac{\beta}{2} \xi^{+-} \right) p^\mp + (p^\pm)^{-1} - \frac{\mu^\pm \xi_{\pm\pm}^2 + \mu^\mp \xi_{\mp\mp}^2}{\beta} = 0, \quad (56)$$

analogous to (34). Now the equation is cubic and the structure of solutions is different. We could not find the solution in the closed form but it is clear that a pair of cubic equations will have either a single solution (p^+, p^-) or nine combinations (p^+, p^-). Numerical analysis of (56) reveals only two inequivalent solutions, analogous to (35), i.e. one of them has a single free energy minimum, the other one a pair of degenerate minima. Therefore, we again have two disordered solutions, one of which is glassy (frustrated).

Now we can write down also the RG equations for the effective action (55). In this calculation we put $\xi_{\alpha\beta}^2 = \sigma_{\alpha\beta}^2 \equiv \sigma^2$ for simplicity. Following the same logic as earlier, the equations are found to be [54]:

$$\begin{aligned} \frac{\partial g}{\partial \ell} &= -8\pi (g + g')^2 y^4 \cosh(2\beta^2 \sigma^2) \cosh(2\beta^2 \sigma^2) - 8\pi (g - g')^2 y^4 \\ \frac{\partial g'}{\partial \ell} &= -\pi (g + g')^2 y^4 \cosh(2\beta^2 \sigma^2) \cosh(2\beta^2 \sigma^2) - \pi (g - g')^2 y^4 \\ \frac{\partial y}{\partial \ell} &= 2\pi (1 - g - g' - \mu_+ - \mu_- - \beta^2 \sigma^2) y \\ \frac{\partial \mu}{\partial \ell} &= -8\pi \mu \\ \frac{\partial \sigma^2}{\partial \ell} &= -2\pi \beta^4 \sigma^4 y^4. \end{aligned} \quad (57)$$

Like in the clean case, the chemical potential is irrelevant and the solutions for fixed point are the same as for the PR beams, including the spin-glass fixed point. We conclude that the phase structure of the optical system is repeated in strongly correlated doped antiferromagnets, which also exhibit the spin-glass phase and have the phase diagram sketched in Fig. 17. In this context it is more interesting to plot the phase diagram in the $\sigma^2 - 1/g$ plane, mimicking the $x - T$ phase diagram of quantum critical systems [33] (remember that the coupling constant g also behaves roughly as inverse temperature in XY-like models). Bear in mind that all phases shown are about vortex dynamics, i.e. one should not compare Fig. 17 to the textbook phase diagram of high-temperature superconductors, which accounts also for the charge or stripe order and the superconducting order. All vortex phases would be located inside the pseudogap regime of the superconductor, where various exotic orders can coexist (assuming, of course, that our model

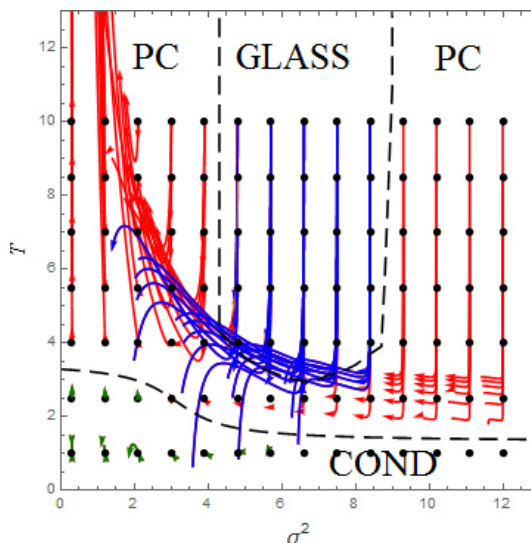


FIG. 17: The phase diagram of the two-sublattice doped Heisenberg antiferromagnet model in the $\sigma^2 - 1/|g'|$ plane, taking into account that $1/g' \sim T$, for $u = r = 1$ and varying v so as to have $g = -0.5$ with varying g' (we have rescaled $\sigma^2 \mapsto 12\sigma^2$). At high temperatures, the vortex conductor becomes either a perfect vortex conductor or a spin glass. Spin glass (blue) is recognized by the fact that the RG equations flow to nonzero disorder at finite and large g' (low temperatures). The PC phase (red) flows toward zero disorder and zero coupling (infinite T), collapsing practically to a single trajectory. The flows for the conductor (green) end up at $T = \sigma^2 = 0$ but are not shown to scale in the figure. Black dashed curves are approximate phase boundaries.

is an adequate approximation of the magnetic order in a cuprate or similar material, which is a complex question). Crucially, the spin-glass phase (blue curves) flows toward *finite disorder* σ^2 , whereas the remaining two phases end up at zero disorder, either at infinite temperature (PC, red flows), or at zero temperature (conductor, green flows). The RG flows in the conductor phase are almost invisible in the figure, as the flows are much slower than in the remaining two phases. As we have shown above, the same phase diagram holds also for the optical system.

1. Discussion

The first papers which found and explored the spin-glass phase in a very similar model are [43–45, 47]. The main difference is that the papers cited consider the spiral (non-collinear) spin order. These works are all inspired by the cuprate materials, the most celebrated brand of high-temperature superconductors. While [44, 45] explore in detail the transport properties, we have no pretension neither to provide a realistic model of cuprates nor to explore in detail all the properties of the spin-glass phase. We are content to see that the PR system of \mathbb{Z} vortices reproduces the phase structure of a certain kind of dirty Heisenberg antiferromagnets (with spatial $O(3)$ spins and \mathbb{Z}_2 vortices), besides the more obvious connection to systems which directly reproduce the \mathbb{Z} vortices in multicomponent $U(1)$ systems like multicomponent Bose-Einstein condensates and type-1.5 superconductors.

VI. CONCLUSIONS

We have investigated the light intensity patterns in a strongly nonlinear optical system, a pair of counterpropagating laser beams in a photorefractive crystal. We have studied this system as a strongly interacting field theory and have focused mostly on the formation and dynamics of vortices. The vortices show a remarkable collective behavior and their patterns are naturally classified in the framework of statistical field theory: the effective action shows several different phases with appropriate order parameters, and the system is essentially an XY model with two flavors, i.e. two kinds of vortex charge, coming from the two beams. The interaction between the flavors is the central reason that the energy of the Coulombic interactions between the two flavors in general cannot be locally minimized at every point. This leads to interesting patterns and behavior. In the presence of disorder, a phase with multiple free energy minima arises, where the absence of long-range order is complemented by the local islands of ordered vortex structure, and which resembles spin glasses.

The reader can notice that the phase diagram is simple in terms of the effective parameters – vortex coupling constants – and quite complex when expressed in terms of the experimentally controllable quantities – the intensity of the laser beams, the intensity of the background photonic lattice and the properties of the photorefractive crystal (the last is not controllable but can be estimated reasonably well [3]). The lesson is that the approach we adopt can save us from demanding numerical work if the space of original parameters is ”blindly” explored. Our phase diagrams can serve as a starting point for ”guided” numerical simulations, suggesting what phenomena one should specifically look for. So far the field-theoretical and statistical approach was not much used in nonlinear optics. We hope to stimulate work in this direction, which is promising also because of the potential of the photorefractive systems to serve as models of strongly correlated condensed matter systems. They make an excellent testing ground for various models because of the availability and relatively low cost of experiments.

In this work we have focused on the relation of the photorefractive counterpropagating system to the model of an $O(3)$ doped antiferromagnet with two sublattices. The authors of previous works on this model [42, 44–46] were motivated mainly by the ubiquitous problem of understanding the pseudogap phase in cuprate superconductors. The applicability of the model to this particular problem is still an open question – it may well be that cuprate physics goes far beyond. But numerous other materials are solid candidates. Here it is mainly an illustration on how one can simulate condensed matter systems in photorefractive optics.

Another field where vortices are found as solutions of a non-linear Schrödinger equation are cold atom systems and Bose-Einstein condensates [16]. Notice however that Bose-Einstein condensates in optical traps are usually (but not always, see [22]) three-dimensional systems with Abrikosov vortex lines, rather than XY-type systems and our formalism would be more complicated there: in three spatial dimensions, vortices give rise to emergent gauge fields already in absence of quenched disorder. The multi-component systems of this kind give rise to so-called type 1.5 superconductors [21] which are a natural goal of further study.

A more complete characterization of the glass-like phase is also left for further work. The reader will notice we have devoted very little attention to the correlation functions in various parameter regimes or the scaling properties of susceptibility, which should further corroborate the glassy character of the system. This is quite difficult in general but very exciting as it offers an opportunity to tune the parameters (e.g., disorder strength) freely in the optical system and study the glass-like phase and its dynamics in real ”time” L , by changing the length of the photorefractive crystal.

Acknowledgments

We are grateful to Mariya Medvedyeva for careful reading of the manuscript. Work at the Institute of Physics is funded by Ministry of Science and Education, under grant no. OI171033.

Appendix A: Perturbation theory and stability analysis

In this section we will develop the perturbation theory of the photorefractive beam system starting from the Lagrangian (4). The perturbation theory yields the criterion for the stability of the intensity patterns as they propagate along the z -axis. Formally, it is just the perturbative diagrammatic calculation of the causal propagator familiar from field theory. This calculation explicitly excludes topologically nontrivial patterns and thus is somewhat peripheral for our main goal, the understanding of the vortex dynamics. But the general ways by which an envelope $\Psi_{F,B}(x, y; z)$ can evolve along the z -axis and become unstable remain valid also for vortices. In particular, we will end up with a classification of geometrical symmetries of the intensity pattern $\Psi^\dagger \Psi$; the same symmetries are seen in vortex patterns and are an important guide for numerical and experimental work – how to recognize instabilities and also phases of the system (see the next section when we come to the description of the phase diagram of the vortex system).

Our system is strongly nonlinear, thus a naive perturbation theory about the ”trivial vacuum”, i.e. constant beam intensity is out of question. The right way is to perturb about a nontrivial solution, which approximates a stable pattern. This means we treat the light intensity as constant in ”time” z but non-constant in space (x, y) . This is the hallmark of spatial dynamical solitons: they propagate with a constant profile along the z -axis and to a good approximation do not interact with each other and do not radiate [3]. We thus write $\Psi = \Psi_0 + \delta\Psi$, giving $\Psi^\dagger \Psi = I_0 + F_0(\delta\Psi_+^\dagger + \delta\Psi_+) + B_0(\delta\Psi_-^\dagger + \delta\Psi_-) + \delta\Psi^\dagger \delta\Psi + O(|\delta\Psi|^2)$ with $F_0^2 + B_0^2 = I_0$. The lowest-order Lagrangian for Ψ_0 now reads

$$\mathcal{L}_0 = \Psi_0^\dagger \Delta \Psi_0 + \Gamma I_0 - \Gamma(1 + \tau u + \tau E_0) \log(1 + \tau u + I_x + I_0), \quad (\text{A1})$$

which determines the shape of the solution $\Psi_0(x, y)$ in the first approximation. Notice the dynamical term with $\partial_z \Psi$ drops out (it is proportional to the equation of motion for Ψ). The expansion of the potential about this solution reads

$$V_{\text{eff}}(\delta\Psi^\pm) = -\Gamma\delta\Psi^\dagger\delta\Psi - \Gamma\frac{1+\tau u+\tau E_0}{2(1+\tau u+I_x+I_0)^2} \times \\ \times \left((\Psi_0\delta\Psi^\dagger)^2 + (\Psi_0^\dagger\delta\Psi)^2 - 2(1+\tau u+I_x+I_0)\delta\Psi^\dagger\delta\Psi - (\Psi_0\sigma_2\delta\Psi^\dagger)(\Psi_0^\dagger\sigma_2\delta\Psi) \right), \quad (\text{A2})$$

so the linearized equation for the fluctuations follows from the Lagrangian quadratic in $\delta\Psi^\dagger, \delta\Psi$:

$$(\pm i\sigma_3\partial_z - q^2 + \Gamma - (1+\tau u+\tau E_0))\delta\Psi^\mp \mp \Gamma\frac{1+\tau u+\tau E_0}{(1+\tau u+I_x+I_0)^2}\delta\Psi^\pm = 0, \quad (\text{A3})$$

where $\delta\Psi^+ \equiv \delta\Psi^\dagger, \delta\Psi^- \equiv \delta\Psi$. In homogenous "spacetime" (z, x, y) we can transform to momentum space in both transverse and longitudinal direction. In the transverse plane we get $(x, y) \mapsto (q_x, q_y)$ and $\Delta \mapsto -q^2$. The longitudinal coordinate or "time" z transforms as $z \mapsto k_n$ where $k_n = \pi n/L$, so the "time" maps to discrete frequencies. The reason is of course that its domain is finite, corresponding to the crystal length L .

Now we can derive the bare propagator (causal Green's function) of the fluctuating dynamical field $\delta\Psi$ by inserting the appropriate source $S(z)$ on the right-hand side of the equation (A3). Normally, the source in the equation for the Green's function is just the Dirac delta function but the counterpropagating nature of our beams imposes a "two-sided" source:

$$S(z) = \begin{pmatrix} \delta(z) & 0 \\ 0 & \delta(z-L) \end{pmatrix}. \quad (\text{A4})$$

With this source (also Fourier-transformed in z), Eq. (A3) gives the bare propagator $G_{\alpha\beta}^{(0)}$ for the fields $\delta\Psi_{\alpha\beta}^\pm$:

$$G^{(0)}(k_n, q) = \frac{-ik_n S(k_n) + \hat{A}^* S(k_n) - \hat{B} S(k_n)}{-k_n^2 - 2i(\Re \hat{A})k_n + \hat{A}^* \hat{A} - \hat{B} \hat{B}^* + [\hat{A}^*, \hat{B}]}. \quad (\text{A5})$$

The auxiliary matrices \hat{A}, \hat{B} defined as follows:

$$\hat{A} = i \begin{pmatrix} p_0 + p_1 - q^2 & p_0 \\ -p_0 & -p_0 - p_1 + q^2 \end{pmatrix}, \quad \hat{B} = i \begin{pmatrix} p_0 & p_0 \\ -p_0 & -p_0 \end{pmatrix}, \quad (\text{A6})$$

where finally $p = (1/4)I_0\Gamma(1+\tau u+\tau E_0)/(1+\tau u+I_x+I_0)^2, p_0 = \Gamma - \Gamma(1+\tau u+\tau E_0)/(1+\tau u+I_x+I_0)$, and $S(k_n) = \text{diag}(1, e^{ik_n L})$.

Now we have the basic ingredient of the perturbation theory – the bare propagator. The self-energy correction of the propagator from the potential V_{eff} can be expanded in a power series over $\delta\Psi^\pm$, which gives an infinite tower of vertices. Simple combinatorial considerations give the expansion

$$\Sigma = \sum_{j_1, j_2, j_3 \in \mathbb{N}} \frac{(-1)^{j_1+j_2+j_3} (j_1+j_2+j_3-1)!}{j_1! j_2! j_3!} \frac{\Gamma(1+\tau u+\tau E_0)}{(1+\tau u+I_0+I_x)^{j_1+j_2+j_3+1}} (\Psi_0^\dagger \delta\Psi)^{j_1} (\Psi_0 \delta\Psi^\dagger)^{j_2} (\delta\Psi^\dagger \delta\Psi)^{j_3}, \quad (\text{A7})$$

and now we can formulate the diagrammatic rules. We have two kinds of propagators, $G^{(0)}$ and its Hermitian conjugate. The mean-field values Ψ_0^\pm are external sources. The term of order (j_1, j_2, j_3) contains $j_1 + j_3$ propagator lines $G^{(0)}$ (out of these j_1 lines ending with the source Ψ_0), and $j_2 + j_3$ lines $(G^{(0)})^\dagger$ (out of these j_2 ending with a source Ψ_0^\dagger). The expansion has to be truncated at some $j_1 + j_2 + 2j_3 \equiv j$. Since the mass dimension of Ψ is 1, the (j_1, j_2, j_3) -diagram has the scaling dimension $2 - 2(j_1 + j_2 + 2j_3) < 0$, so *all* diagrams are irrelevant in the IR. This means we can make a truncation at small j [55]. The leading terms are those where the order of the perturbation in $\delta\Psi^\pm$, which equals $j_1 + j_2 + 2j_3$ is the smallest, giving $j_1 = 1, j_2 = j_3 = 0$ and $j_2 = 0, j_1 = j_3 = 0$. They contain a single external source and introduce the wavefunction renormalization, $G^{(0)} \mapsto ZG^{(0)}$, which does not influence the stability analysis. The four quadratic terms (with $(j_1, j_2, j_3) = (2, 0, 0), (0, 2, 0), (1, 1, 0), (0, 0, 1)$) introduce a mass operator. Only the terms $(1, 1, 0)$ and $(0, 0, 2)$ are trivial (non-interacting); the other two are interacting as they contain $(\delta\Psi^\pm)^2$, and require the calculation of an internal loop, giving the dressed propagator:

$$G^{-1}(k_n, q) = \left(G^{(0)}(k_n, q) \right)^{-1} + \hat{m}^2, \quad (\text{A8})$$

where the mass squared is a *positive* matrix, because their coefficients in (A7) have positive sign (from the term $(-1)^{j_1+j_2+j_3}$ with $j_1 = 2$ or $j_2 = 2$ and the other two indices zero) and the integral of the bare propagator is also positive. Explicitly, it reads

$$\hat{m}^2 = \frac{\Gamma(1 + \tau u + \tau E_0)}{(1 + \tau u + I_0 + I_x)^2} \sum_{k_n} \int_0^\infty dq q G^{(0)}(k_n, q), \quad (\text{A9})$$

where the discrete "frequency" k_n is summed in steps of πL . Other than the mass renormalization, the dressed propagator has the same structure as the bare one. Now we will consider what this means for the stability of the patterns.

1. The pole structure, stability and dispersion relations

Consider the poles of the propagator defined by the zeros of the eigenvalues of the matrix $G_{\alpha\beta}^{-1}(k_n, q)$. The stable solution corresponds to the situation where the perturbation $\delta\Psi_\pm$ dies out (with appropriate boundary conditions), so the stability of the solution is determined by the condition that the pole in q should have a non-positive imaginary part, i.e. that a small perturbation decays. The denominator is quadratic in p_0 which contains the term q^2 , so each of the two eigenvalues λ_\pm defines two pairs of opposite poles, $\pm q_{*+}, \pm q_{*-}, \pm q_{**+}, \pm q_{**-}$. Out of these, two pairs are positive for all parameter values, so we have either two pairs of centrally-symmetric imaginary poles, or one such pair, or none at all. We thus expect the sequence of symmetry-breaking transitions:

$$O(2) \longrightarrow \mathbb{C}_4 \longrightarrow \mathbb{C}_2 \quad (\text{A10})$$

Full circular symmetry is expected when there is no instability. With a single pair of unstable eigenvalues, we expect a square-like pattern with \mathbb{C}_4 symmetry, and with two pairs only a single reflection symmetry axis remains, yielding the group \mathbb{C}_2 . Only in the presence of disorder in the background lattice intensity pattern I_x can we expect the full breaking of the symmetry group down to unity, but this is an *explicit* breaking due to disorder and is not captured by this analysis.

The dispersion relation for a typical choice of parameter values is represented in Fig. 18, where we plot the location of the pole $k(q)$ in the continuous approximation (interpolating between the k_n values), with real parts of the pole in blue and imaginary in red. Since we have two pairs of opposite eigenvalues, the dispersion is P -symmetric in both x, y and z (remember that "time" is really another spatial dimension), and any dispersion relation with a nonzero imaginary part will have a branch in the upper half-plane, i.e. an unstable branch. The only way out of instability is that the pole is purely real, i.e. infinitely sharp – this quasiparticle-like excitation signifies a solitonic solution. In Fig. 18, the dashed lines are drawn with the bare propagator $G^{(0)}$ and the full lines with the dressed propagator G , for the sets of parameter values. The perturbation always reduces the instability, i.e. the magnitude of the imaginary part of the poles – in (A,B) completely, resulting in zero imaginary part, and in (C,D) only partially. This reduction of instability likely explains the fact that linear stability analysis works extremely well for hypergaussian beams (which have most power at small values of q), as found in [28].

The fact that the imaginary region always lies at finite q implies that the instability always starts at a finite scale, which corresponds to the behavior seen in the edge instability, which is shown, e.g., in Fig. 4. In order to understand the central instability, which starts from a single point, corresponding to $q \rightarrow \infty$, one needs to take into account also the higher order corrections from the potential (A7) which, as we discussed, diverge at $q \rightarrow \infty$. While we always have a natural UV cutoff, it may happen that the corrections become large (though finite) before that UV scale is reached. We postpone a detailed account for the subsequent publication, and content ourselves to give only the diagram of the movement of the poles in the complex plane. Higher-order terms bring q -dependent corrections and break the inversion symmetry, resulting in the evolution of poles as in Fig. 19. The instability corresponds to the situations where the poles have an imaginary part, i.e. the first three situations in the figure. The last pattern, with no symmetry at all, is stable, with two real poles.

The analysis performed here is obviously incomplete, and we have contented ourselves merely to give a sketch of how the instabilities considered in the main text arise, as well as to formulate a perturbation scheme which allows one to study such phenomena. Further work along the lines of [28, 31, 32] is possible making use of our formalism, and we plan to address this topic in the future.

[1] M. Cross and P. Hohenberg, *Pattern formation outside of equilibrium*, Rev. Mod. Phys. **65**, 851 (1993).

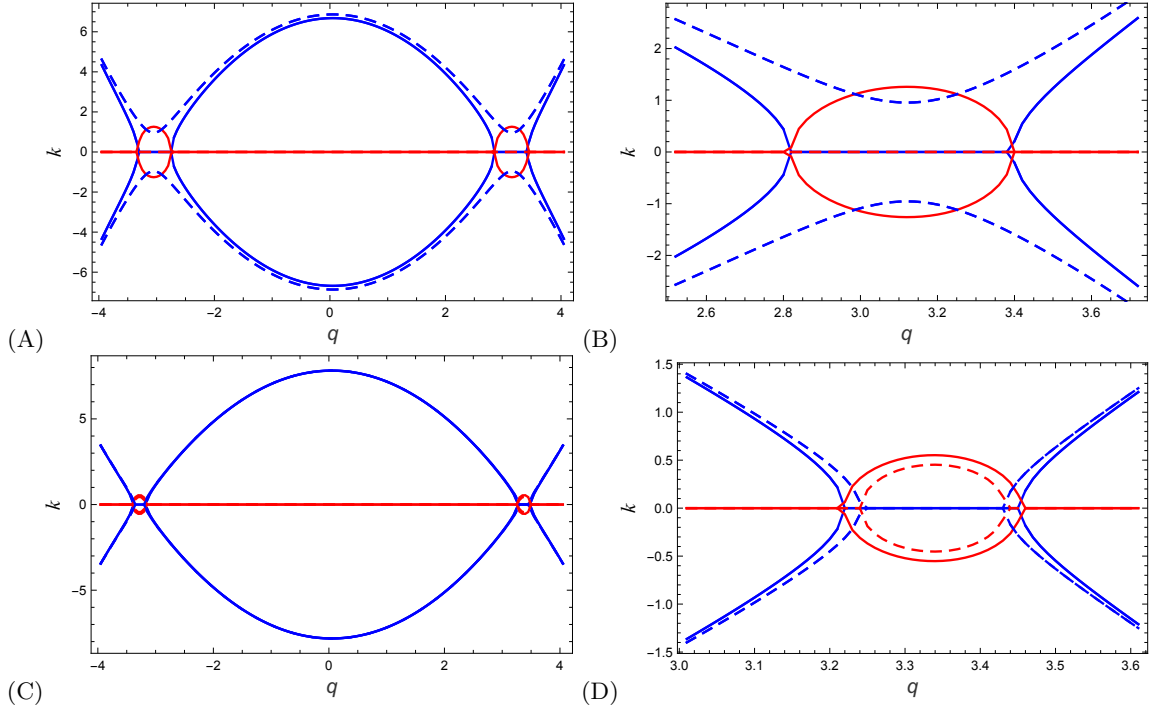


FIG. 18: Dispersion relation (i.e., the position of the poles of the propagator) $k(q)$, where k is the continuous approximation of the discrete effective momentum $k_n = \pi n L$, for $I_0 = 1, I_x = 0$ (A,B) and for $I_0 = 1, I_x = 1$ (C,D), with $\Gamma = 15$ and $L = 10\text{mm}$. The plots (B,D) are zoom-ins from the plots (A,C). Blue lines denote $\Re k$ and red lines $\Im k$. Notice that the propagator contains only k_n^2 and q^2 , so the pole has two copies with opposite sign and is either real or pure imaginary. Dashed lines are the corrected relations, with dressed propagator instead of the bare one. In the top panels, the region of instability, with $\Im k_n \neq 0$, is cured by the nonlinear corrections, whereas in the bottom panels the instability remains. This generically happens at finite q and corresponds to the edge instability.

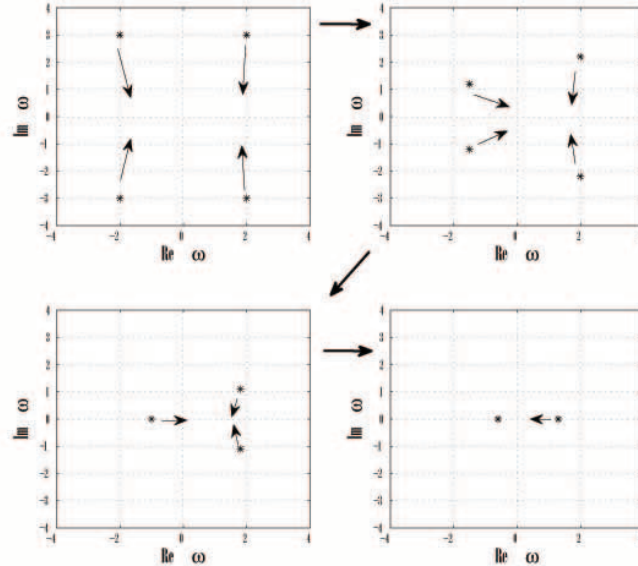


FIG. 19: The movement of the poles in the complex momentum plane in the case of central instability, for $\Gamma = 5, 7, 9, 11$ and $I_0 = I_x = 1, L = 10\text{mm}$. The complex k is denoted by ω . Starting from the \mathbb{C}_4 -symmetric situation with two pairs of complex-conjugate poles, we first break the symmetry down to \mathbb{C}_2 and eventually lose all geometric symmetry as the two pairs merge into two real poles.

- [2] M. I. Rabinovich, A. B. Ezersky and P. D. Weidman, *The Dynamics of Patterns*, (World Scientific, Singapore, 2000).
- [3] C. Denz, M. Schwab and C. Wehnau, *Transverse Pattern Formation in Photorefractive Optics*, (Springer, 2003).
- [4] L. I. Pismen, *Vortices in nonlinear fields*, (Oxford University Press, London, 1999).
- [5] A. Auerbach, *Interacting electrons and quantum magnetism*, (Springer, 1994).
- [6] E. Fradkin, *Field theories of condensed matter systems*, (Addison-Wesley, Redwood City, 1991).
- [7] A. M. Tsvelik, *Quantum field theory in condensed matter physics*, (Cambridge University Press, 2003).
- [8] P. Cvitanović et al, *ChaosBook.org version 15*, chaosbook.org, 2015.
- [9] M. C. Rechtsman, J. M. Zeuner, Y. Plotnik, Y. Lumer, D. Podolsky, F. Dreisow, S. Nolte, M. Segev and A. Szameit, *Photonic Floquet topological insulators*, Nature **496**, 196 (2013). [arXiv:1212.3146[physics]]
- [10] Y. Plotnik, M. Rechtsman, D. Song, M. Heinrich, J. Zeuner, S. Nolte, Y. Lumer, N. Malkova, J. Xu, A. Szameit, Z. Chen and M. Segev, *Observation of unconventional edge states in "photonic graphene"*, Nature Materials **13**, 57 (2014).
- [11] R. Rajaraman, *Solitons and instantons*, (North Holland, Amsterdam 1989).
- [12] M. S. Petrović, M. R. Belić, C. Denz and Yu. S. Kivshar, *Counterpropagating optical beams and solitons*, Lasers Photonic Rev. **5**, 214 (2011). [arXiv:0910.4700[physics.optics]]
- [13] A. A. Abrikosov, *On the magnetic properties of superconductors of the second group*, JTEP **5**, 1174 (1957).
- [14] H. Kleinert, *Gauge fields in condensed matter. Vol I: superflow and vortex lines*, (World Scientific, Singapore, 1989).
- [15] P. W. Anderson, Nature Physics **3**, 160 (2007).
- [16] A. L. Fetter, *Rotating trapped Bose-Einstein condensates*, Rev. Mod.Phys. **81**, 647 (2009).
- [17] J. D. Sau and S. Sachdev, *Mean-field theory of competing orders in metals with antiferromagnetic exchange interactions*, Phys. Rev. B **89**, 075129 (2014). [arXiv:1311.3298[cond-mat]]
- [18] V. L. Berezinsky, Sov. Phys. JETP **32**, 493 (1971); J. Kosterlitz and D. Thouless, J. Phys. C **6**, 1181 (1973).
- [19] E. Babaev, M. Carlstrom, M. Silaev and M. Speight, *Type-1.5 superconductivity in multicomponent systems*, (2016). [arXiv:1608.02211[cond-mat]]
- [20] M. Silaev and E. Babaev, *Microscopic derivation of two-component Ginzburg-Landau model and conditions of its applicability in two-band systems*, Phys. Rev. B **85**, 134514 (2012). [arXiv:1110.1593[cond-mat.supr-con]]
- [21] M. Silaev and E. G. Babaev, *Microscopic theory of type-1.5 superconductivity in multiband systems*, Phys. Rev. B **84**, 094515 (2011). [arXiv:1102.5734[cond-mat.supr-con]]
- [22] X. Ma, R. Driben, B. Malomed, T. Meoer and S. Schumacher, *Two-dimensional symbiotic solitons and vortices in binary condensates with attractive cross-species interaction*, Nature Scientific Reports **6**, 34847 (2016). [arXiv:1606.08579[physics.optics]]
- [23] M. Petrović, D. Jović, M. Belić, J. Schröder, Ph. Jander and C. Denz, *Two dimensional counterpropagating spatial solitons in photorefractive crystals*, Phys. Rev. Lett **95**, 053901 (2005).
- [24] M. Petrović, D. Träger, A. Strinić, M. Belić, J. Schröder and C. Denz, *Solitonic lattices in photorefractive crystals*, Phys. Rev. E **68**, 055601(R) (2003). [arXiv:nlin/0306041]
- [25] M. S. Petrović, D. M. Jović, M. S. Belić and S. Prvanović, *Angular momentum transfer in optically induced photonic lattices*, Phys. Rev. A **76**, 023820 (2007).
- [26] D. M. Jović, S. Prvanović, R. D. Jovanović and M. S. Petrović, *Gaussian induced rotation in periodic photonic lattices*, Opt. Lett. **32**, 1857 (2007).
- [27] M. S. Petrović, *Counterpropagating mutually incoherent vortex-induced rotating structures in optical photonic lattices*, Opt. Exp. **14**, 9415 (2006).
- [28] D. M. Jović, M. S. Petrović and M. R. Belić, *Counterpropagating pattern dynamics: from narrow to broad beams*, Opt. Comm. **281**, 208 (2008).
- [29] M. I. Rodas-Verde, H. Michinel and Y. S. Kivshar, *Dynamics of vector solitons and vortices in two-dimensional photonic lattices*, Opt. Lett. **31**, 607 (2006).
- [30] T. J. Alexander, A. S. Desyatnikov and Y. S. Kivshar, *Multivortex solitons in triangular photonic lattices*, Opt. Lett. **32**, 1293 (2007).
- [31] B. Terhalle, T. Richter, A. S. Desyatnikov, D. N. Neshev, W. Krolikowski, F. Kaiser, C. Denz and Yu. S. Kivshar, *Observation of multivortex solitons in photonic lattices*, Phys. Rev. Lett **101**, 013903 (2008).
- [32] B. Terhalle, T. Richter, K. Law, D. Göries, P. Rose, T. Alexander, P. Kevrekidis, A. Desyatnikov, W. Krolikowski, F. Kaiser, C. Denz and Yu. S. Kivshar, *Observation of double-charge discrete vortex solitons in hexagonal photonic lattices*, Phys. Rev. A **79**, 043821 (2009).
- [33] Sachdev S. *Quantum phase transitions* (Cambridge University Press, 1999).
- [34] N. D. Mermin, Rev. Mod. Phys. **51**, 591 (1979).
- [35] J. Cardy, *Scaling and renormalization in statistical physics* (Cambridge University Press, 1996).
- [36] M. Mezard, G. Parisi, M. A. Virasoro, *Spin glass theory and beyond*, (World Scientific, Singapore, 1987).
- [37] T. Castellani and A. Cavagna, *Spin-glass theory for pedestrians*, J. Stat. Mech. **05**, P05012, (2005). [arXiv:cond-mat/0505032]
- [38] J. L. Cardy and S. Ostlund, *Random symmetry-breaking fields and the XY model*, Phys. Rev. B **25**, 6899 (1982).
- [39] A. Perret, Z. Ristivojevic, P. Le Doussal, G. Schehr and K. Wiese, *Super-rough glassy phase of the random field XY model in two dimensions*, Phys. Rev. Lett. **109**, 157205 (2012). [arXiv:1204.5685[cond-mat.dis-nn]]
- [40] C. A. Bolle, V. Aksyuk, F. Pardo, P. L. Gammel, E. Zeldov, E. Bucher, R. Boie, D. J. Bishop and D. R. Nelson, *Observation of mesoscopic vortex physics using micromechanical oscillators*, Nature **399**, 43 (1999).
- [41] S. Bogner, T. Emig, A. Taha and C. Zeng, *Test of replica theory: Thermodynamics of two-dimensional model systems with quenched disorder*, Phys. Rev. B **69**, 104420 (2004). [arXiv:cond-mat/0309145]

- [42] J. Zaanen, *Quantum phase transitions in cuprates: stripes and antiferromagnetic supersolids*, Physica C **317**, 217 (1999). [arXiv:cond-mat/9811078]
- [43] N. Hasselmann, A. H. Castro Neto and C. Morais Smith, *Spin glass phase of cuprates*, Phys. Rev. B **69** 014424 (2003). [arXiv:cond-mat/0306721] [arXiv:cond-mat/0512528]
- [44] V. Juričić, L. Benfatto, A. O. Caldeira and C. Morais Smith, *Dissipative dynamics of topological defects in frustrated Heisenberg spin systems*, Phys. Rev. B **71**, 064421 (2005). [arXiv:cond-mat/0410082]
- [45] V. Juričić, L. Benfatto, A. O. Caldeira and C. Morais Smith, *Dynamics of topological defects in a spiral: a scenario for the spin-glass phase of cuprates*, Phys. Rev. Lett **92**, 137202 (2004). [arXiv:cond-mat/0510312[cond-mat.dis-nm]]
- [46] L. Benfatto, M. Silva-Neto, V. Juričić and C. Morais Smith, *Derivation of the generalized nonlinear sigma model in the presence of the Dzyaloshinskii Moriya interaction*, Physica B **378**, 449 (2006).
- [47] V. Juričić, M. B. Silva-Neto and C. Morais Smith, *Lightly Doped as a Lifshitz Helimagnet*, Phys. Rev. Lett. **96** 077004 (2006).
- [48] A. del Maestro, B. Rosenow and S. Sachdev, *From stripe to checkerboard ordering of charge-density waves on the square lattice in the presence of quenched disorder*, Phys. Rev. B **74**, 4520, (2006). [arXiv:cond-mat/0603029]
- [49] One specificity of multi-component vortices is that the coupling constants may be negative, as can be seen from (9). In that case the ordering of the four regimes (how they follow each other upon dialing L) changes but the overall structure remains.
- [50] Nevertheless, this is clearly not a rigorous argument. Our mean-field calculation is somewhat sketchy and merely assumes that the long-range interactions can safely be modeled as a uniform vortex charge field.
- [51] They are distinct from the bifurcations which happen also in topologically trivial beam patterns and lead to the instability of (non-topological) solitons. These instabilities have been analyzed in the Appendix and in more detail in [28], where the authors have found them to start from the edge of the beam and result in the classical "walk through the dictionary of patterns".
- [52] As a rule, it follows the sequence (A10) found in the Appendix from the pole structure of the propagator, though some of the steps can be absent, e.g. for a single Gaussian vortex there is no \mathbb{C}_2 stage.
- [53] One could also enforce the constraint exactly, through the nonlinear sigma model, as was done in [43]. While the leading term of the vortex Hamiltonian would remain the same in that case, the amplitude fluctuations have different dynamics which influences the terms of the vortex Hamiltonian RG flow (though probably not the very existence of the glass phase).
- [54] For the most general case of different and non-scalar matrices $\sigma_{\alpha\beta}^2$ and $\xi_{\alpha\beta}^2$ the flow equations for them complicate significantly and we will not consider them.
- [55] Remember we do not worry about the UV divergences: we have an effective field theory and the UV cutoff is physical and finite.